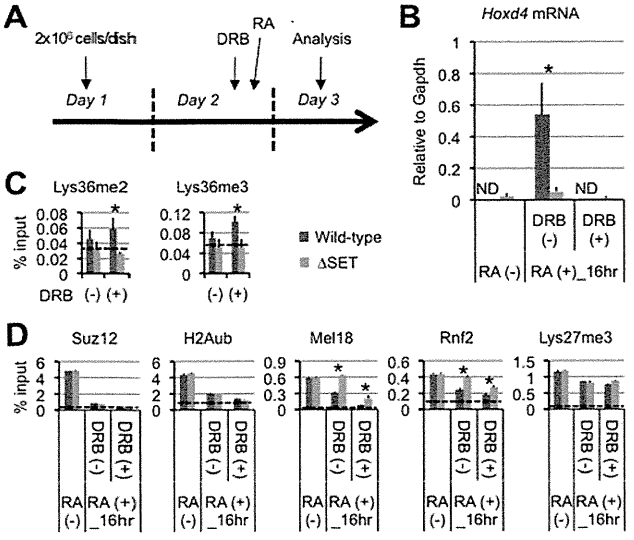

Figure 5. Lys36me2/3 and exclusion of the PRCs occur independently of productive transcriptional elongation. (**A**) Protocol for RA-induced differentiation of ES cells under DRB pretreatment. DRB was added to the culture medium 1 hour before the addition of RA, then the ES cells were cultured for another 16 hours in the presence of 100 nM RA. (**B**) Nuclear run-on assay in combination with RT-qPCR analyses of *Hoxd4* mRNA expression either with or without DRB pretreatment. The results are represented as values relative to *Gapdh* mRNA in each cell type. Error bars represent s.d. (Student's t-test, *P<0.05). ND: not detected. (**C** and **D**) ChIP assays of differentiating ES cells either with (+) or without (−) DRB pretreatment. A promoter-proximal coding region of *Hoxd4* was analyzed. The antibodies used are indicated above each graph. The results are represented as means and s.d. (Student's t-test, *P<0.05). Broken lines indicate approximate levels of ChIP signals in either *Il2ra* promoter (C) or *Gapdh* coding region (D) as controls.
doi:10.1371/journal.pgen.1003897.g005

and then the cells were cultured for another 16 hours in the presence of RA (Figure 5A).

Under these conditions, *Hoxd4* mRNA was not increased at all from the basal level that was observed in undifferentiated ES cells, indicating that DRB blocked the productive transcriptional elongation completely (Figure 5B). As shown in Figure 5C, while wild-type ES cells displayed mild increases in Lys36me2/3 levels in the promoter-proximal coding region of *Hoxd4* in response to DRB, ΔSET ES cells did not, resulting in clear differences between wild-type and ΔSET ES cells in the presence of DRB. The results indicate that Ash1l-dependent Lys36me2/3 in *Hoxd4* occurs independently of productive transcriptional elongation during the establishment of transcriptional activation. This may be reasonable since Ash1l is preloaded on the *Hoxd4* chromatin before the addition of RA (see Figure 3E).

Ash1l promotes exclusion of the PRC1 in a transcription-independent manner

Can transcription-independent Lys36me by Ash1l counteract Polycomb silencing? A previous report showed that transcription is necessary to exclude the PRCs from local chromatin [23]. However, proof remains elusive of whether progression of RNAPII itself is the major determinant factor for the exclusion. Moreover, how the PRCs are removed upon gene induction is poorly understood. Therefore, under the same conditions, i.e. the addition of DRB prior to RA, we characterized the status of Polycomb silencing in ES cells by analyzing Suz12 (a component of the PRC2), Lys27me3 (an enzymatic product of the PRC2), ubiquitination of histone H2A (H2Aub, an enzymatic product of the PRC1), Mel18, and Rnf2 (components of the PRC1) in *Hoxd4* chromatin.

We found significantly higher levels of Mel18 and Rnf2 in *Hoxd4* chromatin of ΔSET ES cells compared to wild-type cells in the absence and presence of DRB (Figure 5D). Interestingly, wild-type and ΔSET ES cells displayed clear decreases in Mel18 and Rnf2 levels upon blocking of transcription by DRB, demonstrating anti-parallel ChIP patterns against those of Lys36me2/3 (compare Figures 4A, 5C and 5D). Similar results were obtained for a distal coding region of *Hoxd4* (Figure S6C). Suz12 and H2Aub levels showed more rapid and clear decreases in response to RA. However, differences between wild-type and ΔSET ES cells in the occupancies of Suz12 and H2Aub were unclear, suggesting that there was an Ash1l-independent pathway to exclude these molecules. Lys27me3 levels displayed only a marginal response to both DRB and RA under these conditions (Figure 5D). However, we observed a clear decrease in Lys27me3 levels after a longer induction by RA, in which there was a substantial difference between wild-type and ΔSET ES cells (Figure S6D).

In summary, these experiments showed that Suz12, H2Aub, Mel18 and Rnf2 demonstrated relatively rapid responses to RA compared with Lys27me3, and contradicting a previous notion, their exclusion was not dependent on transcriptional elongation. Importantly, we found that exclusion of Mel18 and Rnf2 from chromatin upon RA induction was specifically impaired by loss of the methyltransferase activity of Ash1l, suggesting a negative relationship between PRC1 chromatin association and Ash1l activity. Although ΔSET ES cells displayed mild decreases in RNAPII Ser2-phosphorylation (Ser2p) levels in the coding regions of *Hoxd4*, the decreased levels of Lys36me did not affect the basic status of RNAPII for the most part (Figures S7A–S7C). Similar results were obtained even for a relatively larger gene, *Wnt6* (Figures S7D and S7E). These results suggest that the methyltransferase activity of Ash1l mainly contributes to promoting the anti-Polycomb silencing function rather than the activation of RNAPII directly.

The functional link between Lys36me and Lys16ac in an entire coding region

Having established that Lys36me in *Hoxd4* occurs independently of productive transcriptional elongation and that DRB enhances the difference between wild-type and ΔSET ES cells, we next asked how the Lys36me facilitates transcriptional elongation. Given that certain histone acetylations have more direct effects on activation of transcription, ChIP assays were performed to analyze the effects of Lys36me on representative histone acetylations, such as Lys9/14 acetylation of H3 (Lys9/14ac) and Lys16 acetylation of H4 (Lys16ac). In all subsequent experiments, when necessary, DRB was added during RA treatment as in Figure 4.

Interestingly, the ChIP pattern of Lys16ac in *Hoxd4* was similar to that of Lys36me in that the ChIP signals were not decreased in the presence of DRB. In fact, they were increased in wild-type ES cells, and became clearly lower in ΔSET ES cells compared with wild-type cells (Figure 6A), thereby revealing the effect of Lys36me by DRB. The ChIP pattern of Lys9/14ac did not resemble even slightly that of Lys36me. These results collectively indicate that Lys16ac specifically correlates with Ash1l-dependent Lys36me, both of which are independent of RNAPII Ser2p. This was consistent with a recent report conducted in *Drosophila*, where connections were made between Lys36me2 with dMes-4 and

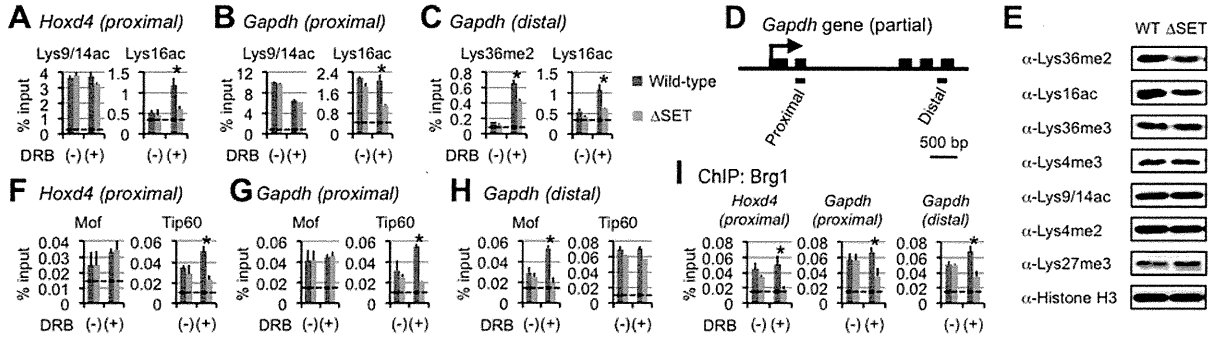

Figure 6. Functional links of Ash1l to the Tip60, Mof, and Brg1 complexes. (**A–C** and **F–I**) ChIP assays of *Hoxd4* and *Gapdh* in differentiating ES cells either with (+) or without (−) DRB treatment. Regions that were analyzed were divided into two parts as indicated in each panel: promoter-proximal (*proximal*) and distal (*distal*) coding regions. The antibodies used are indicated above each graph or in panels. The results are represented as means and s.d. (Student's t-test, *P<0.05). Broken lines indicate approximate levels of ChIP signals in *Il2ra* promoter as a control. (**D**) A diagram of the *Gapdh* gene is shown. Black bars under the diagram indicate the regions analyzed by ChIP assays. (**E**) Whole-cell extracts were analyzed by immunoblot using the antibodies against the indicated histone modifications.
doi:10.1371/journal.pgen.1003897.g006

Lys16ac by an unknown enzyme in proximal coding regions [24]. Interestingly, in our study, similar results were also obtained for *Gapdh* (Figure 6B), even in a further downstream distal coding region (Figures 6C and 6D), suggesting that cooperative action between Lys36-methylases including Ash1l and a certain Lys16 acetyltransferase influences these histone modifications in an entire coding region independently of RNAPII Ser2p. Similar results were obtained for *Hoxb4* and *Hprt1* (Figure S8), suggesting that the observed parallel link is a general phenomenon. In ΔSET ES cells, the global levels of Lys36me2 and Lys16ac, but not of Lys36me3, were found to be reduced (Figure 6E), which further corroborated the ChIP results.

The Tip60 and Mof complexes are co-regulated with Lys36me in a region-dependent manner

Since we observed no significant difference in the levels of Ash1l, RNAPII, and Ser5p between wild-type and ΔSET ES cells (see Figure 4A), we speculated that Lys36me contributed to the association of a certain Lys16-acetyltransferase with a coding region chromatin. We next analyzed the Mof and Tip60 complexes as these complexes preferentially acetylate Lys16 of histone H4 and are highly relevant to transcriptional activation. Furthermore, since these complexes contain chromodomain proteins (Msl3l [25] in the Mof complex and Mrg15 [26] in the Tip60 complex) that bind Lys36-methylated histone H3 [27,28], both complexes can associate with the Lys36-methylated chromatin. The ChIP patterns of Tip60 in the promoter-proximal coding region of *Hoxd4* and *Gapdh* were similar to those of Lys16ac, while Mof showed distinct patterns (Figures 6F and 6G). However, in the distal coding region of *Gapdh*, the ChIP pattern of Mof was similar to that of Lys16ac (Figure 6H), while the similarity in that of Tip60 became less prominent. These results suggest that both Tip60 and Mof are the enzymes that acetylate Lys16 downstream of Ash1l-dependent Lys36me and that they differentially associate with a target gene in a region-dependent manner, i.e. Tip60 in a promoter-proximal coding region and Mof in a distal coding region. The involvement of the acetyltransferase activity of Tip60 in *Hoxd4* activation was further suggested by utilizing *Tip60* knock-in mutant ES cells (heterozygote) (Figure S9). Under these conditions, Lys36me2 was likely to be affected, suggesting crosstalk between Ash1l and Tip60.

Interplay with Brg1, a key factor for chromatin reprogramming, is revealed by DRB

Having demonstrated functional interaction between Lys36me by Ash1l and Lys16ac by Tip60 or Mof, we then analyzed other events that the interaction influences. Among the chromatin remodeling complexes associated with gene activation, several *in vitro* studies suggest that the Brg1 complex is the most plausible candidate that targets Lys16ac [29,30], although whether this applies *in vivo* remains unclear. The ChIP pattern of Brg1 in the promoter-proximal coding region of *Hoxd4* was mostly similar to those of Lys36me and Lys16ac (Figure 6I, left panel). We observed a similar result for *Gapdh* (Figure 6I, middle panel), even in the distal coding region (Figure 6I, right panel). Next, as the active P-TEFb complex containing both Cdk9 and Brd4 has been shown to target Lys16ac [31], we also analyzed the occupancy of Cdk9. However, the ChIP pattern of Cdk9 showed only a limited similarity to those of Lys36me and Lys16ac (data not shown). Therefore, these results suggest that Lys36me by Ash1l contributes to Brg1 association in an entire coding region.

Ash1l is required for a proper response to a certain activating cue during development

We next examined whether our results in ES cells could be recapitulated in development of mice. Whole-mount *in situ* hybridization was employed to determine expression patterns of representative Hox genes in various parts of developing embryos that carry the ΔSET mutation. While the expression patterns of *Hoxb4*, *d4*, and *a4* mRNAs were largely similar between wild-type and ΔSET embryos, the anterior boundaries of their expression domains were shifted posteriorly along the antero-posterior axis at the paraxial mesoderm in ΔSET embryos (Figures 7, S10A and S10B). Thus, consistent with the results in ES cells, these findings suggest that the methyltransferase activity of Ash1l promotes a response to a certain activating cue that triggers Hox gene expression during development.

A genetic interaction between *Ash1l* and *Mel18* in a skeletal phenotype

To examine whether the observed posterior shifts of the expression domains of *Hoxb4* and *Hoxd4* mRNAs are reflected by skeletal phenotype, we compared vertebrae of wild-type and mutant mice. Consistent with Ash1l being one of the trithorax

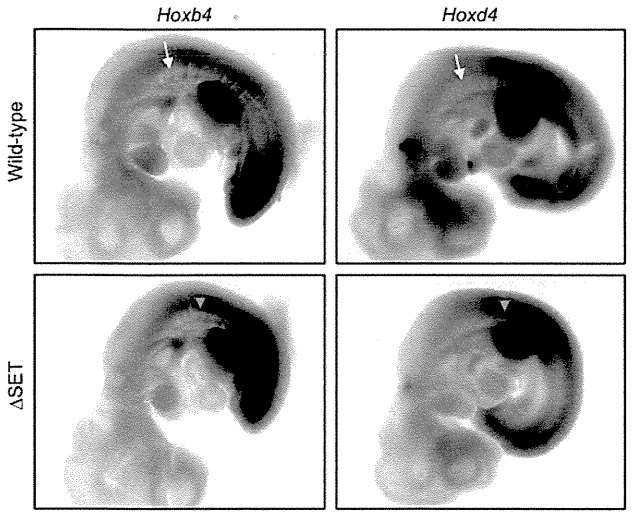

Figure 7. Posterior shifts of the expression boundaries of *Hoxb4* and *Hoxd4* mRNAs. Whole-mount *in situ* hybridization analyses of *Hoxb4* and *Hoxd4* mRNA expression in E10.5 embryos. Shown are normal (white arrows) and affected (orange arrow-heads) anterior expression boundaries at the paraxial mesoderm in wild-type and ΔSET mutant embryos, respectively.
doi:10.1371/journal.pgen.1003897.g007

group proteins, obvious alterations in the identities of vertebrae were observed (Table 1, Figures 8A and S10C–S10I). In particular, 42–56% of the mutant mice had cervical vertebrae affected, showing the homeotic transformation of the C2 vertebra into the C1 vertebra. These phenotypes were similar to those caused by mutations in group 4 Hox genes, since the C2-to-C1 transformation was caused by a functional loss of either *Hoxb4* or *Hoxd4* [32], which support our results in ES cells and embryos. Importantly, we found that the ΔSET allele partially suppressed the C2-to-C3 transformation caused by homozygous mutations in *Mel18*, indicating a role for Ash1l in anti-Polycomb silencing *in vivo* (Figure 8B).

Discussion

In contrast to prevalent notions, at least with regards to Hox gene activation, the present study has shown that both Lys36me2/3 in a coding region and the accompanying exclusion of the PRCs from the region occur independently of productive transcriptional elongation. RNA-Seq analysis revealed a significant functional relationship between Ash1l and Polycomb-regulated genes in that Ash1l-mediated Lys36me counteracts Polycomb silencing. Intriguingly, ChIP-Seq analysis has suggested that the preceding Lys36me2/3 during the establishment of Hox gene expression is applicable to a subset of RAR-associated genes. We have also uncovered a functional link among Ash1l, Tip60, Mof, and Brg1, which cooperatively promote Hox gene expression in response to RA. Collectively, our results reveal insights into mechanisms underlying the establishment of transcriptional memory that counteracts Polycomb silencing, which have until now been difficult to analyze by conventional methods.

Here, we propose that Ash1l and RAR coordinate to orchestrate a novel regulatory cascade of chromatin reprogramming (Figure 9). The Lys36me2/3 preceding productive transcriptional elongation may directly counteract association of the PRCs in target chromatin [33,34], resulting in de-repression from Polycomb silencing, likely through loosening of the compacted chromatin structure [35]. Therefore, Lys36me2/3 by Ash1l and other Lys36-methylases constitute a rate-limiting step, which may promote Lys16ac by Tip60 or Mof in a region-dependent manner. Lys16ac may lead to further loosening of the chromatin structure [29], allowing the Brg1 chromatin remodeling complex to be associated and to promote chromatin reprogramming, presumably by further excluding the PRCs to alleviate Polycomb silencing and by remodeling nucleosomes to facilitate productive transcriptional elongation.

The proposed mechanism might be also applied to transcriptional regulation in the *Drosophila* species, showing a correlation between Lys36me2 and Lys16ac [24]. Indeed, the consecutive regulatory steps described above might explain a previous report detailing progression of the ecdysone-induced puff 74EF in polytene chromosomes of *Drosophila* larvae under pretreatment with DRB [36]. However, the mechanism would not apply in yeast, in which an anti-correlation between Lys36me2 and histone H4 acetylation has been reported [20,21]. These observations suggest that such regulatory mechanisms are unique to metazoans.

What is the significance of Lys36me3 during the establishment of transcriptional activation? At least in a promoter-proximal coding region of *Hoxd4*, we found Lys36me3 could occur independently of productive transcriptional elongation (Figure 5C). An accumulation of Lys36me3 on the Lys36me2-platform may ensure de-repression from Polycomb silencing because Lys36-demethylases Kdm2a/b would not recognize Lys36me3 as a substrate [33]. The degree of Lys36-trimethylase recruitment was presumably RA-dependent as we observed only a small increment in the level of Lys36me3 in the presence of DRB in B16 cells without addition of RA (Figure S5). A predisposition to underrepresent RAR-associated genes in the "decreased" gene groups in response to DRB as well as accumulations of Lys36me2/3 around RAR binding sites further support our surmise (Figures 4G and 4H). Of note, DRB clearly increased the Lys36me2/3 levels in promoter-proximal coding regions of *Hoxb4/d4* in ΔSET ES cells (Figures 4A and S4B). Therefore, we speculate that several Lys36-methylases, including Ash1l, play a role during the establishment of transcriptional activation in an RA-dependent manner. Consistent with this speculation, Ash1l, Nsd1, and a major mammalian Lys36-trimethylase Setd2, all have a nuclear receptor binding motif, L*XX*LL. Indeed, approximately 60% of RAR binding sites were co-occupied with Ash1l (Figure S1G). Thus, it is tempting to speculate that nuclear receptor-dependent developmental programs may have similar underpinnings to the Hox genes regulator mechanisms revealed in this study.

Our results suggest that a part of the function of Lys36me2/3 in *Hoxd4* mRNA expression is masked after productive transcriptional elongation. Specifically, the effect of Lys36me2/3 on the association with Tip60 and Brg1 was more evident in the presence of DRB (Figures 6F–6I), suggesting that this association is partially dependent on P-TEFb activity. Once the active P-TEFb complex associates with target chromatin and triggers the productive transcriptional elongation, it may have a dominant effect on the association over that of Lys36me2/3. However, upon gene activation but before tethering of the P-TEFb complex, Lys36me2/3 may have a dominant comprehensive function, involving exclusion of the PRCs and promoting association of Tip60 and Brg1, thereby facilitating the RA response (Figure 9). This idea is consistent with our results demonstrating that sensitivity against a certain activating cue appeared to be affected in ΔSET mice and ES cells (Figures 1F, 7, S10A and S10B).

One of the important issues when studying transcription mechanisms on a chromatin template is how a dramatic change

Table 1. Skeletal phenotypes observed in progenies by intercrossing of heterozygotes.

Region and type of abnormalities		Genotypes		
		+/+	+/ΔSET	ΔSET/ΔSET
Cervical region				
C1	Fusion of the anterior arch of atlas to the dens of C2	0	6 (17%)	5 (20%)
	Incomplete ventral arch (right side)	0	2 (6%)	2 (8%)
C2	Broadened neural arch (C2 to C1)	0	15 (42%)	14 (56%)
C4–C7	Fusion of the neural arch (C4 and C5/C5 and C6)	0	1 (3%)	1 (4%)
	Ectopic rib from C7 (C7 to T1)	0	1 (3%)	3 (12%)
Thoracic region				
	T1 to C7	0	1 (3%)	0
	Abnormal rib cage	0	2 (6%)	1 (4%)
Lumbar region				
	L6 to S1	0	2 (6%)	0
Total number affected		0	19 (53%)	20 (80%)
Total number unaffected		12 (100%)	17 (47%)	5 (20%)
Total number analyzed		12	36	25

doi:10.1371/journal.pgen.1003897.t001

in chromatin structure occurs upon gene activation: in particular, whether the open chromatin structure is established before or after the first RNAPII travels along the template DNA [37]. So far, it is widely believed that a specially equipped RNAPII, or so-called "pioneer polymerase", is required for the initial opening of the condensed chromatin. This special RNAPII breaks down the condensed chromatin structure into the open structure during the first transcriptional elongation, thereby ultimately creating the transcription-competent chromatin. However, the results of the present study led us to the notion that the driving forces initiated by the methyltransferase activity of Ash1l promote the establishment of the open and transcription-competent chromatin structure prior to the first productive transcriptional elongation by fully-activated RNAPII. Our hypothesis may be applied to active but

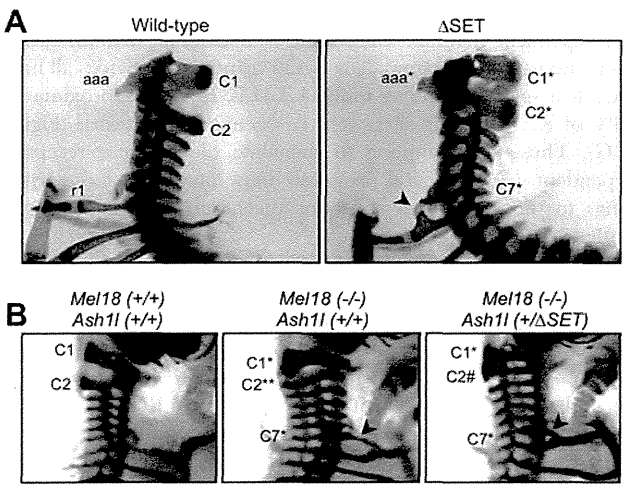

Figure 8. Typical skeletal phenotypes of *Ash1l* ΔSET mice, and a genetic interaction between *Ash1l* and *Mel18*. Lateral views of the cervico-thoracic region of the axial skeleton are shown. (**A**) The C2-to-C1 transformation in a ΔSET mouse (C2*), deformities of the anterior arch of the atlas (aaa* at C1*) and an ectopic rib (arrow-head) on the C7 vertebra (C7*). (**B**) A genetic interaction between *Mel18* mutant allele and *Ash1l* ΔSET allele. The C2-to-C3 transformation (C2**) in a *Mel18* mutant mouse is partially suppressed by an additional *Ash1l* ΔSET allele (C2#).
doi:10.1371/journal.pgen.1003897.g008

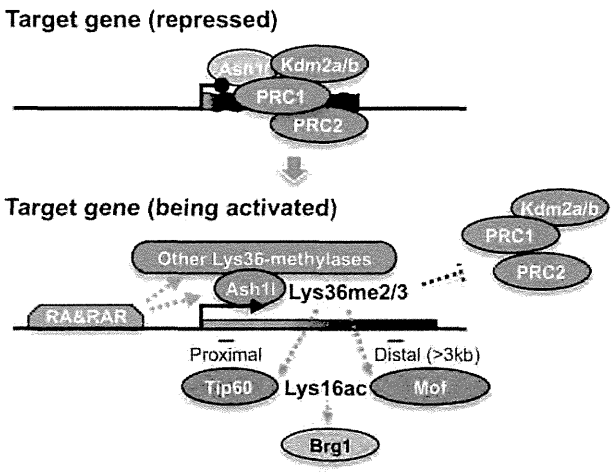

Figure 9. A proposed role of Ash1l with RAR in the establishment of transcriptional activation. In the upper panel, Ash1l is preloaded in the promoter-proximal coding region with the condensed bivalent chromatin (thick and short gene body) that mainly generates immature short transcripts (represented in orange on the gene body). Enzymatic activity of Ash1l is inactivated under the condition (light-red). During the establishment of transcriptional activation, retinoic acid and its receptor (RA&RAR) promote activation of Ash1l (dark-red), as well as association of the other Lys36-methylases with the target chromatin. These Lys36-methylases, including Ash1l, orchestrate the downstream mechanisms directly or indirectly, thereby further promoting RA response through alleviating the repressive effect of the PRCs and opening the condensed chromatin (represented by the extended shape of the gene body in the bottom panel) independently of transcriptional elongation. The Brg1 complex may indirectly target Lys36me2/3 through Lys16ac.
doi:10.1371/journal.pgen.1003897.g009

non-productive bivalent genes; however, it remains unclear whether it can be applied to inactive, inducible monovalent genes.

Results from whole-mount *in situ* hybridization analyses in *Ash1l* ΔSET mice (Figures 7, S10A and S10B) were clearly distinct from those in mutant mice carrying a deletion in the SET domain of Mll1, a representative Lys4-methylase belonging to the trithorax group, which displayed a normal expression boundary and an impaired maintenance of *Hoxd4* mRNA expression [38]. On the other hand, the results in *Ash1l* ΔSET mice were similar to those in the Polycomb group mutant mice in that the mutants demonstrated shifts of expression boundaries at the paraxial mesoderm (*Mel18* in [39]; *Phc1/2* in [40]), although directions of the shifts in Polycomb group mutant mice were opposite to those in *Ash1l* ΔSET mice. Collectively, these results suggest that Ash1l has a distinct function from Mll1 and directly counteracts the function of the Polycomb group proteins. Consistent with this idea, *Ash1l* ΔSET mice only demonstrated additive and non-synergistic phenotypes with the double-heterozygous *Mll1* mutation [YY & KN, unpublished observation], and a partial suppression in the phenotype with the *Mel18* mutation (Figure 8B).

We also observed that Ash1l was localized in a promoter-proximal coding region (Figures 3E, 3F and S1E), corroborating previous reports [8,9]. Bromo-, PHD- and BAH-domains in the carboxyl-terminal region of Ash1l supposedly function to restrict localization. The distribution of Ash1l in *Hoxd4* was similar to those of Lys4me2/3, and a large portion of Ash1l was co-localized with Lys4-methylated chromatin (Bivalent and Lys4me alone, Figure S1F). It is tempting to speculate that the specific localization of Ash1l may be necessary for certain interaction partners of Ash1l, such as Ly4-trimethylases, to be recruited in a promoter-proximal coding region. Of note, we also found that Ash1l was clearly present in the absence of RA (Figure 3E) and in genes that were not expressed (Figures S1F and S1G). Surprisingly, it appeared that the methyltransferase activity of Ash1l was inactive under these conditions. Presumably, Ash1l is deposited but poised to achieve an immediate action in response to RA. It remains unclear how the enzymatic activity of Ash1l protein is activated. Future studies on the Ash1l complex and its interaction partners, as well as using knockout mice, may resolve these issues.

Unexpected is the increase in the level of Lys36me2 upon DRB treatment. It is possible that, under normal conditions, there may be a competition for methylation sites between Lys36-trimethylase Setd2 and other Lys36-dimethylases including Ash1l. In the presence of DRB, the lack of transcription-dependent trimethylation by Setd2 would result in a spreading of Lys36me2 catalyzed by the dimethylases. In a subset of RAR-associated genes, the Lys36-trimethylase, accompanied with RAR, may generate Lys36me3 on the plat-form of accumulated Lys36me2 in a transcription-independent manner. This may explain the increased levels of Lys36me2/3 upon DRB treatment in the subset of RAR-associated genes including *Hoxd4*.

In this study, using an Ash1l mutant and DRB, we have revealed a novel function for Ash1l during the establishment of transcriptional activation of Polycomb-regulated genes, including Hox and Wnt family genes. Given that the Wnt signaling pathway integrates numerous environmental signals *in vivo*, Ash1l may modulate a variety of signals in many biological processes. We have also found novel functional links among several chromatin modifiers that reprogram the status of target chromatin. Future studies on these factors will provide further insights into precise mechanisms for the establishment of transcriptional memory that counteracts Polycomb silencing of developmentally regulated genes.

Materials and Methods

Ethics statement

The animals' care was in accordance with institutional guidelines of National Institute of Genetics in Japan and Saga University Faculty of Medicine.

Generation of *Ash1l* ΔSET mice

The schematic representation of the strategy used for targeted disruption of mouse *Ash1l* gene is shown in Figure 1A. A targeting vector was constructed by insertion of DNA fragments of introns 10–12 (5′SphI-SpeI) of mouse *Ash1l* gene into a ploxFNFDT-SS backbone vector, in which 5′BamHI-3′SphI fragment was replaced to a PCR-cloned floxed exon fragment (exons 11–12) with a Pgk-Neo^r cassete. PCR primer-pairs used for the cloning are listed in Table S4. ΔSET mice were generated with M1 ES cells (derived from *F1* of C57BL/6J and 129/Sv), and backcrossed to C57BL/6J between two to six times. Genotypes were determined by PCR using the primer-pairs listed in Table S4.

Generation and characterization of polyclonal antibodies against mouse Ash1l protein

cDNA encoding a part of Ash1l protein (2803–2891, Figure S1C) was inserted into the bacterial expression vector pGEX 6P-1 (GE Healthcare). The PCR primer-pairs used are listed in Table S4. GST-fusion proteins were induced and were purified using glutathione-sepharose beads. The eluates containing the recombinant proteins were pooled and dialyzed against PBS. The antibodies were raised against each GST-fusion protein and affinity-purified. Since endogenous Ash1l protein was difficult to detect by immunoblot, the specificity of the antibodies was checked by immunofluorescence analysis under transient expression of lentiviral-mediated shRNA directed against mouse *Ash1l* mRNA (Figure S1D). Pseudovirus was produced from HEK293T cells by cotransfection of packaging plasmids (Addgene) and pRSI9 vector (Cellecta, Decipher Project) using PEI-MAX (Polysciences). The target sequence in *Ash1l* mRNA was following: 5′-GCCAAAUUCUCCUUCUCAUUU-3′.

Cell cultures

ES cells were cultured on gelatin-coated dishes in a basic culture medium of KO-DMEM (Gibco) containing 1× GlutaMAX-I (Gibco), 1× MEM NEAA (Gibco), 0.1 mM 2-mercaptoethanol (Gibco), 50 units/ml penicillin (Gibco), 50 μg/ml streptomycin (Gibco), without feeder cells. For culturing undifferentiated ES cells, the above basic culture medium was supplemented with 1,000 units/ml of leukemia inhibitory factor (LIF) (Chemicon), 15% Knockout Serum Replacement (Invitrogen), and 1% fetal calf serum (Gibco), and 10 mM 4-(2-hydroxyethyl)-1-piperazineethanesulfonic acid (Hepes) buffer. For culturing differentiating ES cells, only 10% fetal calf serum (Gibco) was supplemented to the above basic culture medium. A typical protocol for cell culture is shown in Figure 1D, in which RA is added to the differentiation medium at indicated time points. DRB (Sigma) was added at a final concentration of 75 μM on either Day 3 or Day 4 (16 hour-exposure) before analysis.

ChIP assays

Chromatin immunoprecipitation was performed according to online protocols provided by Millipore (for histone modifications) or Abcam (for the other proteins) with modifications in fixation protocols. The antibodies and fixation protocols used are listed in Table S5. Immunoprecipitated DNA was purified using a PCR

Purification Kit (Qiagen), and was quantified by real-time PCR using SYBR green dye on a LightCycler480 machine (Roche). PCR temperatures for acquisitions of DNA amplification signals were determined empirically. PCR primer-pairs used are listed in Table S4. Background signals are shown in Figure S11A and are subtracted from most of the respective results. Control ChIP signals in either a promoter-proximal coding region of *Gapdh* or a promoter region of *Il2ra* are indicated in relevant figures (Figure S11B). Unless otherwise stated, each result and error bar in graphs represent mean and s.d., respectively, of three independent PCR reactions from a single ChIP experiment that is representative of several that were performed (3 to 5 experiments).

ChIP-Seq and data analysis

For ChIP-Seq, $1–5\times10^7$ ES cells were used and chromatin was sheared to an average DNA fragment size of 150–250 bp. After immunoprecipitation using Dynabeads protein G (Invitrogen), ChIP-Seq libraries were prepared according to Illumina protocols. The libraries were sequenced using an Illumina HiSeq 1000. All ChIP-Seq reads were mapped to the mouse genome (mm9) using Bowtie2 with default parameters. Genomic profiles were generated using igvtools and were viewed in Integrative Genomics Viewer (IGV). Peaks of Ash1l and RAR ChIP-Seq signals on genome were determined using MACS2 with false-discovery rate as 0.05. Each associated gene for the peaks was determined using Entrez gene annotation with in-house computer program, in which Ash1l-target genes were defined as genes containing Ash1l-peaks around transcription start site (TSS) within +/−4 kb and RAR-associated genes were defined as genes containing RAR-peaks in up-stream (from −20 kb to TSS) and coding regions. Datasets for reads/kb/million mapped (RPKM) values of Lys36me2/3 in coding regions of each gene were normalized to 75th percentile. Raw sequencing data were submitted to the NCBI Short Read Archive database under accession number (GSE48421). Mouse ES cell RAR ChIP-Seq datasets (GSE19409) [22] were downloaded from the NCBI Short Read Archive database and were compared with Lys36me2/3 datasets generated by our study.

In situ RNA hybridization

Hox cDNAs were RT-PCR-cloned from embryonic total RNA into pBluescript. Primer-pairs used for PCR amplification are listed in Table S4. Single-stranded RNA probes labeled with either [^{35}S]-UTP (for section) or digoxigenin-UTP (for whole-mount) were synthesized according to manufacturer's instructions (Promega; Roche). *In situ* hybridization was performed according to the procedures described previously [41,42]. After hybridization and washing, the sections were immersed in Kodak NBT emulsion (diluted 1:1 with 2% glycerol), exposed for 2 weeks and developed in a Kodak D-19 developer. For whole-mount *in situ* hybridization, probes were detected using alkaline phosphatase-conjugated anti-digoxigenin Fab fragment (Roche) and signals were developed using Nitro blue tetrazolium chloride (NBT) and 5-Bromo-4-chloro-3-indolyl phos- phate, toluidine salt (BCIP) (Roche).

Skeletal analysis

Skeletal preparations were prepared from perinatal mice as described previously [41]. Cartilage and ossified bone were stained with alcian blue-alizarin red.

Nuclear run-on assays

The run-on transcription assay was performed as described previously with following modifications [43]. Briefly, $5–7\times10^6$ cells were treated with ice-cold hypotonic nuclei isolation buffer (20 mM Hepes-KOH [pH 7.6], 10 mM NaCl, 5 mM $MgCl_2$, 0.5% NP-40, 1 mM DTT, 0.2 mM PMSF, 1 mM Bezamidine-HCl) and the isolated nuclei were re-suspended in storage buffer (50 mM Hepes-KOH [pH 7.6], 0.1 mM EDTA, 5 mM $MgCl_2$, 40% glycerol) to give a total 30 µl for each reaction. Transcription was re-started by addition of 30 µl of transcription buffer (10 mM Hepes-KOH [pH 7.6], 0.3 M KCl, 4 mM DTT), 40 units of RNase inhibitor, 3 µl of Biotin RNA Labeling Mix (Roche). The reaction was incubated at 30°C for 45 min on a vortex mixer. After DNase I (Takara) treatment, total RNA was isolated using Isogen II (Nippongene) and 10–20 µg of total RNA was subjected to further purification of nascent RNA molecules using 50 µl of Dynabeads MyOne Streptavidin T1 (Invitrogen) in Click-iT Nascent RNA Capture Kit (Invitrogen). Complementary DNAs were synthesized from purified nascent RNA molecules by on-beads reverse transcription according to the manufacturer's instructions, and the cDNAs were subjected to real-time PCR analyses.

RNA-Seq and data analysis

Total RNA was prepared using Isogen II (Nippongene) and subjected to DNase I (Takara) treatment and further purified by aid of RNeasy Mini Kit column (Qiagen). The poly(A)-containing mRNA were purified and libraries were prepared according to Illumina TruSeq RNA protocols. Data were obtained with the Illumina HiSeq 1000 sequencing machine. All RNA-Seq reads were mapped to the mouse genome (mm9) using TopHat2. Transcript abundance was quantified using Cufflinks and annotations from Ensembl release 70, and FPKM (fragments/kb of transcript/million fragments mapped) values were calculated. To minimize dispersion effect by low-FPKM values, all the FPKM values were modified by addition of 0.1 in log2 transformation. For a classification of chromatin signature, a supplementary table and ChIP-Seq data in Mikkelsen, et al. [18] were used as references. Gene ontology analysis for biological process of the selected genes was performed using Partek Genomic Suite (Ryoka systems). Raw sequencing data were submitted to the NCBI Short Read Archive database under accession number (GSE48419).

Remaining materials and methods including the method for histone methyltransferase assay are available in Text S1.

Supporting Information

Figure S1 Characterization of *Ash1l* gene product (mRNA expression and genomic distribution of Ash1l protein). (**A**) Northern blot analysis of *Ash1l* mRNA expression using total RNA from various adult tissues and whole embryos. (**B**) Conventional RT-PCR analyses of *Ash1l* mRNA expression levels in undifferentiated or differentiated ES cells, developing embryos (E8.5, 10.5, 14.5) and embryonic fibroblasts (MEFs). As controls, expression levels of *Oct4*, *Hoxd4*, and *Gapdh* mRNAs are shown. After RA was added to the culture medium at a final concentration of 1 µM in the absence of LIF and feeder cells, ES cells were further cultured for 4 days. (**C** and **D**) Characterization of the antibodies against Ash1l protein. Rabbit polyclonal antibodies were raised against the carboxyl-terminal region of mouse Ash1l protein (an arrow in C, see Materials and Methods). Immunofluorescence analysis of Ash1l protein in mouse embryonic fibroblasts (D). A lentivirus vector expressing shRNA directed against *Ash1l* mRNA was constructed, and a recombinant virus was infected to mouse embryonic fibroblasts. The virus-infected fibroblasts were labeled by TagRFP. Nuclei were labeled by DAPI. The empty vector was used as a shRNA-negative control. (**E**) Distribution of Ash1l ChIP-Seq read counts relative to

TSS in ES cells. (**F**) Pie chart showing relative ratio of status of chromatin signatures [18] for Ash1l-target genes. (**G**) Venn diagrams showing the relationship of Ash1l-target genes with either Lys4me-positive genes [Lys4me3 (+)], expressed genes (Expressed, FPKM values from RNA-Seq analysis over 0.1), or RAR-associated genes [RAR (+)]. The numbers of genes in each compartment are shown. The total number of annotated genes analyzed was 18,724.
(TIF)

Figure S2 RNA-Seq data for Hox and Wnt family genes in differentiating ES cells. (**A** and **B**) The results of Hox (A) and Wnt (B) family genes were plotted on the graphs using modified FPKM values. The x-axis corresponds to expression levels of each gene (shown as log2 transformation of each FPKM value plus 0.1), and the y-axis corresponds to fold change in gene expression levels between ΔSET ES cells and wild-type (shown as Δlog2 transformation). (**C**) Quantitative RT-PCR analyses of *Hoxd4*, *Wnt6*, and *Gapdh* mRNAs in differentiating ES cells to verify the RNA-Seq results.
(TIF)

Figure S3 RNA-Seq data for marker gene expression. The results of indicated marker genes are plotted on the graphs using modified FPKM values. The x-axis corresponds to expression levels of each gene (shown as log2 transformation of each FPKM value plus 0.1), and the y-axis corresponds to fold change in gene expression levels between ΔSET ES cells and wild-type cells (shown as Δlog2 transformation). (**A**) Undifferentiated ES cells. (**B**) Differentiating ES cells.
(TIF)

Figure S4 ChIP assays of histone modifications for *Hoxb4* and *Hprt1* in differentiating ES cells. (**A**) Diagrams of *Hoxb4* and *Hprt1* genes. Black boxes represent exons. (**B–D**) ChIP assays of histone modifications and the status of RNAPII in differentiating ES cells either with (+) or without (−) DRB treatment. The antibodies used are indicated at the top of each graph. The results are represented as means and s.d. (B) The promoter-proximal coding region of *Hoxb4* was analyzed. (C) The promoter-proximal coding region of *Hprt1* was analyzed. (D) The distal coding region of *Hprt1* was analyzed.
(TIF)

Figure S5 Comparison of DRB-response between ES cells and B16 cells. (**A**) Quantitative RT-PCR analyses of *Hoxd4* and *Gapdh* mRNAs in differentiating ES cells and a melanoma cell line, B16. ES cells were cultured in the presence of RA (see the culture protocol shown in Figure 1D). *Hoxd4* was constitutively active in B16 cells without addition of RA. The left panel depicts expression of *Hoxd4* mRNA in the presence (+) or absence (−) of DRB. The right panel depicts expression of *Gapdh* mRNA. The results are represented as the means and s.d. of three independent PCR reactions. (**B**) RA-dependent increases in Lys36me2/3 levels of *Hoxd4* chromatin in response to DRB. ChIP assays of B16 cells and differentiating ES cells either with (green bars) or without (black bars) DRB treatment. The promoter-proximal coding region of *Hoxd4* in each cell was analyzed. The antibodies used are indicated at the top of each graph. The results are represented as means and s.d.
(TIF)

Figure S6 Exclusion of the PRCs occurs in a transcription-independent manner. ChIP assays of Lys27me3 and Mel18 in differentiating ES cells either with (+) or without (−) DRB treatment. (**A**) Occupancies of Lys27me3 and Mel18 in the promoter-proximal coding region of *Hoxd4* before addition of RA. (**B** and **C**) DRB was added to the culture medium prior to RA, resulting in induction over 16 hours. The promoter-proximal (B) and distal (C) coding regions of *Hoxd4* were analyzed. In (B), the same dataset as in Figure 5D was used. (**D**) RA was added to the culture medium prior to DRB as shown in Figure 1D, resulting in induction over 48 hours. The antibodies used are indicated at the top of each graph. The results are represented as means and s.d.
(TIF)

Figure S7 The status of RNAPII is mostly unaffected in ΔSET ES cells. (**A** and **B**) ChIP assays of various regions of *Hoxd4* in differentiating ES cells before (A) or after (B) addition of RA. The results are represented as relative values that were obtained by normalizing each result to *Gapdh* in each cell type. Error bars represent s.d. of three independent ChIP experiments. The antibodies used are indicated above each graph. Broken lines show approximate levels of ChIP signals in the *Il2ra* promoter. We found that RNAPII was relatively enriched in the promoter-proximal region even before *Hoxd4* activation (A), demonstrating one of the features of promoter-proximal pausing of the poised RNAPII. After RA treatment, the RNAPII levels in the coding regions were increased in both wild-type and ΔSET ES cells to a similar extent (B), suggesting that the recruitment and progression of RNAPII were not affected in ΔSET ES cells. Similar results were obtained with the phosphorylation levels of Ser2 (Ser2p) and Ser5 (Ser5p) at the carboxyl-terminal domain of RNAPII; however, the Ser2p levels in the coding regions of ΔSET ES cells were observed to be slightly affected (B). (**C**) A diagram of the *Hoxd4* gene. Black and grey boxes represent exons and a 3′ RARE, respectively. Black bars under the diagram indicate the regions analyzed by ChIP assays. TSS: transcription start site. (**D**) ChIP assays of promoter-proximal and distal coding regions of *Wnt6* in differentiating ES cells. The results are represented as relative values that were obtained by normalizing each result to *Gapdh* in each cell type. Error bars represent the s.d. of three independent ChIP experiments. The antibodies used are indicated above each graph. Broken lines show approximate levels of ChIP signals in the *Il2ra* promoter. (**E**) A diagram of the *Wnt6* gene. Black boxes represent exons. Black bars under the diagram indicate the regions analyzed by ChIP assays.
(TIF)

Figure S8 ChIP assays of histone H4 Lys16 acetylation for *Hoxb4* and *Hprt1* in differentiating ES cells. Diagrams of *Hoxb4* and *Hprt1* genes are shown on top of each ChIP result. Black boxes represent exons. ChIP assays were performed using differentiating ES cells either with (+) or without (−) DRB treatment. The results are represented as means and s.d. (**A**) The promoter-proximal coding region of *Hoxb4* was analyzed. (**B**) The promoter-proximal (left) and distal (right) coding region of *Hprt1* was analyzed.
(TIF)

Figure S9 Generation of *Tip60* knock-in mutant ES cells. (**A**) Schematic representation of the strategy used for targeted replacement of exon 10 in the *Tip60* gene. The mutated exon 10 encoding a part of the histone acetyltransferase domain with its flanking introns was floxed by loxP sequences. FLPe-mediated recombination resulted in the generation of the mutated allele (Q325E and G328E, heterozygote). Red bars represent mutations in exon 10. (**B**) RT-PCR analysis of RA-induced *Hoxd4* mRNA expression. (**C**) ChIP assays of histone modifications in differentiating ES cells either with (+) or without (−) DRB treatment. The promoter-proximal coding region of *Hoxd4* was analyzed. The antibodies used are indicated at the top of each graph. The results are represented as means and s.d. Likely due to the heterozygosity

of the knock-in mutation, we observed a mild difference in the levels of Lys16ac between wild-type and knock-in mutant ES cells.
(TIF)

Figure S10 *In vivo* analyses of *Ash1l* ΔSET mutant mice. (**A** and **B**) In situ hybridization analysis of *Hoxa4* mRNA in E11.5-embryos. In (A), results of whole-mount in situ hybridizations for *Hoxa4* mRNA are shown. Normal (white arrows) and affected (orange arrowheads) anterior expression boundaries at the paraxial mesoderm in wild-type and ΔSET embryos. In (B), results of in situ hybridizations for *Hoxa4* mRNA are shown in a representative cross-sectional image. A radio-isotope-labeled antisense-riboprobe was used for the detection of the mRNA. Yellow lines represent boundaries between each pre-vertebra (pv). Each arrow indicates the most anterior boundaries of *Hoxa4* mRNA expression. An atrial chamber of the heart in each embryo is encircled by a blue-broken line. (**C**–**H**) Typical skeletal phenotypes of *Ash1l* ΔSET mice. Ventral views of the axial skeleton are shown. (C, D and E) Wild-type, (F, G, and H) ΔSET mice. (**C** and **F**) The cervical region. In (F), the dens of the C2* is fused to the C1*, affecting the formation of the anterior arch of atlas (aaa*). (**F** and **G**) The thoracic region. In (G), the abnormal rib cage is shown. Identities of sternoclavicular joints are mismatched between the left and right sides (for example, r2 to r1*). (**E** and **H**) The lumbo-sacral region. In (H), the transverse process of the L6* is fused to that of the S1. (**I**) Schematic representation summarizing the homeotic transformations. The vertebrae are numbered serially from the C1 vertebra, in which the cervical region is from 1 to 7, the thoracic region is from 8 to 20, the lumbar region is from 21 to 26, and the sacral region is from 27 to 30. a, the C2-to-C1 transformation. b, the C7-to-T1 transformation. c, the T1-to-C7 transformation. d, the L6-to-S1 transformation.
(TIF)

Figure S11 Background and control signals in ChIP assays. (**A**) Background ChIP signals in the promoter-proximal regions of indicated genes with (+) or without (−) DRB treatment are shown. The fixatives that were used are indicated above each graph (see Table S5 for fixation protocols). The results are represented as the means. Most background ChIP signals were around 0.01% input and are subtracted from most of the respective results. (**B**) Control ChIP signals in either a promoter-proximal coding region of *Gapdh* (for Lys27me3, Mel18, Suz12, H2Aub, and Rnf2) or a promoter region of *Il2ra* (for the others). ChIP assays were performed using indicated antibodies and approximate levels of each result are indicated in relevant figures.
(TIF)

Table S1 Results from intercrossing of Ash1l ΔSET heterozygote. Each offspring obtained by mating heterozygotes was genotyped around 3 to 4 weeks after birth by allele-specific PCR using the primers listed in Table S4.
(XLSX)

Table S2 RA-responsive genes and ΔSET-impaired genes. Listed are 543 genes with a value over 2.5 following Δlog2 transformation of modified FPKM values in wild-type ES cells after 10 nM RA treatment for 2 days (WT+RA) over those of undifferentiated cells (WT). Raw FPKM values are shown here. Genes that were down-regulated in ΔSET ES cells are indicated as "Yes" in column F.
(XLSX)

Table S3 Dys-regulated genes in undifferentiated ES cells. Listed are 116 genes that showed changes in expression levels in undifferentiated wild-type and ΔSET ES cells. Raw FPKM values are shown here. Genes that were down-regulated in ΔSET ES cells are indicated as "Down" (59 genes), while genes that were up-regulated in the cells are indicated as "Up" (57 genes) in column D.
(XLSX)

Table S4 Oligonucleotides used in this study. PCR primers and their sequences are listed. All oligonucleotides were synthesized by Hokkaido System Science Co., Ltd.
(XLSX)

Table S5 Antibodies used in this study. These antibodies were used for immunoblots and ChIP assays, in which amounts used for each experiment were empirically determined. Fixative conditions for ChIP assays are shown in column C.
(XLSX)

Text S1 Supplemental Materials and Methods. Remaining materials and methods are described here.
(DOCX)

Acknowledgments

We thank T. Shiroishi for his support with mice breeding; T. Koide for providing the backbone vector for the targeting construct; J. Nakayama for reagents and useful information; R. Gohara for an assistance of gene ontology analysis; K. Isono, H. Oda, D. Reinberg, K. Ura, T. Urano, A. Vaquero, J.L. Workman and Y. Yamaguchi for their critical reviews of the manuscript; and H. Soejima's lab members for helpful discussion.

Author Contributions

Conceived and designed the experiments: KN. Performed the experiments: HM KH YY JS TAE TK MM YK KN. Analyzed the data: HM KH YY JS TAE KN. Contributed reagents/materials/analysis tools: MN. Wrote the paper: KN. Providing general support for this work: SH HK HH HS.

References

1. Guenther MG, Levine SS, Boyer LA, Jaenisch R, Young RA (2007) A chromatin landmark and transcription initiation at most promoters in human cells. Cell 130: 77–88.
2. Cheng B, Price DH (2007) Properties of RNA polymerase II elongation complexes before and after the P-TEFb-mediated transition into productive elongation. J Biol Chem 282: 21901–21912.
3. Gilmour DS (2009) Promoter proximal pausing on genes in metazoans. Chromosoma 118: 1–10.
4. Chiba K, Yamamoto J, Yamaguchi Y, Handa H (2010) Promoter-proximal pausing and its release: Molecular mechanisms and physiological functions. Exp Cell Res 316: 2723–2730.
5. Rahl PB, Lin CY, Seila AC, Flynn RA, McCuine S, et al. (2010) c-Myc regulates transcriptional pause release. Cell 141: 432–445.
6. Mavrich TN, Jiang C, Ioshikhes IP, Li X, Venters BJ, et al. (2008) Nucleosome organization in the Drosophila genome. Nature 453: 358–362.
7. Simon JA, Kingston RE (2009) Mechanisms of polycomb gene silencing: knowns and unknowns. Nat Rev Mol Cell Biol 10: 697–708.
8. Papp B, Müller J (2006) Histone trimethylation and the maintenance of transcriptional ON and OFF states by trxG and PcG proteins. Genes Dev 20: 2041–2054.
9. Gregory GD, Vakoc CR, Rozovskaia T, Zheng X, Patel S, et al. (2007) Mammalian ASH1L is a histone methyltransferase that occupies the transcribed region of active genes. Mol Cell Biol 27: 8466–8479.
10. Beisel C, Imhof A, Greene J, Kremmer E, Sauer F (2002) Histone methylation by the Drosophila epigenetic transcriptional regulator Ash1. Nature 419: 857–862.
11. Tanaka Y, Katagiri Z, Kawahashi K, Kioussis D, Kitajima S (2007) Trithorax-group protein ASH1 methylates histone H3 lysine 36. Gene 397: 161–168.
12. Cabianca DS, Casa V, Bodega B, Xynos A, Ginelli E, et al. (2012) A long ncRNA links copy number variation to a polycomb/trithorax epigenetic switch in FSHD muscular dystrophy. Cell 149: 819–831.
13. Krogan NJ, Kim M, Tong A, Golshani A, Cagney G, et al. (2003) Methylation of histone H3 by Set2 in Saccharomyces cerevisiae is linked to transcriptional elongation by RNA polymerase II. Mol Cell Biol 23: 4207–4218.

14. Li B, Howe L, Anderson S, Yates JR 3rd, Workman JL (2003) The Set2 histone methyltransferase functions through the phosphorylated carboxyl-terminal domain of RNA polymerase II. J Biol Chem 278: 8897–8903.
15. Xiao T, Hall H, Kizer KO, Shibata Y, Hall MC, et al. (2003) Phosphorylation of RNA polymerase II CTD regulates H3 methylation in yeast. Genes Dev 17: 654–663.
16. Kuzin B, Tillib S, Sedkov Y, Mizrokhi L, Mazo A (1994) The Drosophila trithorax gene encodes a chromosomal protein and directly regulates the region-specific homeotic gene fork head. Genes Dev 8: 2478–2490.
17. Rozovskaia T, Tillib S, Smith S, Sedkov Y, Rozenblatt-Rosen O, et al. (1999) Trithorax and ASH1 interact directly and associate with the trithorax group-responsive bxd region of the Ultrabithorax promoter. Mol Cell Biol 19: 6441–6447.
18. Mikkelsen TS, Ku M, Jaffe DB, Issac B, Lieberman E, et al. (2007) Genome-wide maps of chromatin state in pluripotent and lineage-committed cells. Nature 448: 553–560.
19. Tanaka Y, Kawahashi K, Katagiri Z-I, Nakayama Y, Mahajan M, et al. (2011) Dual Function of Histone H3 Lysine 36 Methyltransferase ASH1 in Regulation of Hox Gene Expression. PLoS ONE 6(11): e28171.
20. Carrozza MJ, Li B, Florens L, Suganuma T, Swanson SK, et al. (2005) Histone H3 methylation by Set2 directs deacetylation of coding regions by Rpd3S to suppress spurious intragenic transcription. Cell 123: 581–592.
21. Keogh MC, Kurdistani SK, Morris SA, Ahn SH, Podolny V, et al. (2005) Cotranscriptional set2 methylation of histone H3 lysine 36 recruits a repressive Rpd3 complex. Cell 123: 593–605.
22. Mahony S, Mazzoni EO, McCuine S, Young RA, Wichterle H, et al. (2011) Ligand-dependent dynamics of retinoic acid receptor binding during early neurogenesis. Genome Biol 12: R2.
23. Schmitt S, Prestel M, Paro R (2005) Intergenic transcription through a polycomb group response element counteracts silencing. Genes Dev 19: 697–708.
24. Bell O, Wirbelauer C, Hild M, Scharf AN, Schwaiger M, et al. (2007) Localized H3K36 methylation states define histone H4K16 acetylation during transcriptional elongation in Drosophila. EMBO J 26: 4974–4984.
25. Smith ER, Cayrou C, Huang R, Lane WS, Côté J, et al. (2005) A human protein complex homologous to the Drosophila MSL complex is responsible for the majority of histone H4 acetylation at lysine 16. Mol Cell Biol 25: 9175–9188.
26. Hayakawa T, Ohtani Y, Hayakawa N, Shinmyozu K, Saito M, et al. (2007) RBP2 is an MRG15 complex component and down-regulates intragenic histone H3 lysine 4 methylation. Genes Cells 12: 811–826.
27. Zhang P, Du J, Sun B, Dong X, Xu G, et al. (2006) Structure of human MRG15 chromo domain and its binding to Lys36-methylated histone H3. Nucleic Acids Res 34: 6621–6628.
28. Larschan E, Alekseyenko AA, Gortchakov AA, Peng S, Li B, et al. (2007) MSL complex is attracted to genes marked by H3K36 trimethylation using a sequence-independent mechanism. Mol Cell 28: 121–133.
29. Shogren-Knaak M, Ishii H, Sun JM, Pazin MJ, Davie JR, et al. (2006) Histone H4-K16 acetylation controls chromatin structure and protein interactions. Science 311: 844–847.
30. Singh M, Popowicz GM, Krajewski M, Holak TA (2007) Structural ramification for acetyl-lysine recognition by the bromodomain of human BRG1 protein, a central ATPase of the SWI/SNF remodeling complex. Chembiochem 8: 1308–1316.
31. Zippo A, Serafini R, Rocchigiani M, Pennacchini S, Krepelova A, et al. (2009) Histone crosstalk between H3S10ph and H4K16ac generates a histone code that mediates transcription elongation. Cell 138: 1122–1136.
32. Horan GS, Ramírez-Solis R, Featherstone MS, Wolgemuth DJ, Bradley A, et al. (1995) Compound mutants for the paralogous hoxa-4, hoxb-4, and hoxd-4 genes show more complete homeotic transformations and a dose-dependent increase in the number of vertebrae transformed. Genes Dev 9: 1667–1677.
33. Lagarou A, Mohd-Sarip A, Moshkin YM, Chalkley GE, Bezstarosti K, et al. (2008) dKDM2 couples histone H2A ubiquitylation to histone H3 demethylation during Polycomb group silencing. Genes Dev 22: 2799–2810.
34. Yuan W, Xu M, Huang C, Liu N, Chen S, et al. (2011) H3K36 methylation antagonizes PRC2-mediated H3K27 methylation. J Biol Chem 286: 7983–7989.
35. Francis NJ, Kingston RE, Woodcock CL (2004) Chromatin compaction by a polycomb group protein complex. Science 306: 1574–1577.
36. Ashburner M (1972) Ecdysone induction of puffing in polytene chromosomes of Drosophila melanogaster. Effects of inhibitors of RNA synthesis. Exp Cell Res 71: 433–440.
37. Orphanides G, Reinberg D (2000) RNA polymerase II elongation through chromatin. Nature 407: 471–475.
38. Terranova R, Agherbi H, Boned A, Meresse S, Djabali M (2006) Histone and DNA methylation defects at Hox genes in mice expressing a SET domain-truncated form of Mll. Proc Natl Acad Sci U S A 103: 6629–6634.
39. Akasaka T, Kanno M, Balling R, Mieza MA, Taniguchi M, et al. (1996) A role for mel-18, a Polycomb group-related vertebrate gene, during the anteroposterior specification of the axial skeleton. Development 122: 1513–2215.
40. Isono K, Fujimura Y, Shinga J, Yamaki M, O-Wang J, et al. (2005) Mammalian polyhomeotic homologues Phc2 and Phc1 act in synergy to mediate polycomb repression of Hox genes. Mol Cell Biol 25: 6694–6706.
41. Kessel M, Gruss P (1991) Homeotic transformations of murine vertebrae and concomitant alteration of Hox codes induced by retinoic acid. Cell 67: 89–104.
42. Wilkinson DG, Nieto MA (1993) Detection of messenger RNA by in situ hybridization to tissue sections and whole mounts. Methods Enzymol 225: 361–373.
43. Patrone G, Puppo F, Cusano R, Scaranari M, Ceccherini I, et al. (2000) Nuclear run-on assay using biotin labeling, magnetic bead capture and analysis by fluorescence-based RT-PCR. Biotechniques 29: 1012–1014, 1016–1017.

Journal of Human Genetics (2013) 58, 402–409

www.nature.com/jhg

REVIEW

Epigenetic and genetic alterations of the imprinting disorder Beckwith–Wiedemann syndrome and related disorders

Hidenobu Soejima and Ken Higashimoto

Genomic imprinting is an epigenetic phenomenon that leads to parent-specific differential expression of a subset of genes. Most imprinted genes form clusters, or imprinting domains, and are regulated by imprinting control regions. As imprinted genes have an important role in growth and development, aberrant expression of imprinted genes due to genetic or epigenetic abnormalities is involved in the pathogenesis of human disorders, or imprinting disorders. Beckwith–Wiedemann syndrome (BWS) is a representative imprinting disorder characterized by macrosomia, macroglossia and abdominal wall defects, and exhibits a predisposition to tumorigenesis. The relevant imprinted chromosomal region in BWS is 11p15.5, which consists of two imprinting domains, *IGF2/H19* and *CDKN1C/KCNQ1OT1*. BWS has five known causative epigenetic and genetic alterations: loss of methylation (LOM) at KvDMR1, gain of methylation (GOM) at H19DMR, paternal uniparental disomy, *CDKN1C* mutations and chromosomal rearrangements. Opposite methylation defects, GOM and LOM, at H19DMR are known to cause clinically opposite disorders: BWS and Silver–Russell syndrome, respectively. Interestingly, a recent study discovered that loss of function or gain of function of *CDKN1C* also causes clinically opposite disorders, BWS and IMAGe (intrauterine growth restriction, metaphyseal dysplasia, adrenal hypoplasia congenita, and genital anomalies) syndrome, respectively. Furthermore, several clinical studies have suggested a relationship between assisted reproductive technology (ART) and the risk of imprinting disorders, along with the existence of trans-acting factors that regulate multiple imprinted differentially methylated regions. In this review, we describe the latest knowledge surrounding the imprinting mechanism of 11p15.5, in addition to epigenetic and genetic etiologies of BWS, associated childhood tumors, the effects of ART and multilocus hypomethylation disorders.
Journal of Human Genetics (2013) **58,** 402–409; doi:10.1038/jhg.2013.51; published online 30 May 2013

Keywords: assisted reproductive technology; Beckwith–Wiedemann syndrome; DNA methylation; genomic imprinting; IMAGe syndrome; multilocus hypomethylation disorders; Silver–Russell syndrome

INTRODUCTION

Genomic imprinting is an epigenetic phenomenon that leads to parent-specific differential expression of a subset of mammalian genes. So far, >100 imprinted genes have been identified in humans and mice, and most imprinted genes often form clusters, or imprinting domains. The expression of imprinted genes within these domains is regulated by imprinting control regions (ICRs).[1,2] ICRs are identical to differentially methylated regions (DMRs), which are characterized by DNA methylation on one of the two parental alleles, or maternally methylated DMRs and paternally methylated DMRs. In addition, there are two classes of imprinted DMRs, gametic DMRs and somatic DMRs. Gametic DMRs acquire DNA methylation during gametogenesis, and the methylation is maintained from zygote to somatic cells during all developmental stages. Most gametic DMRs are identical to ICRs. Methylations of somatic DMRs are established during early embryogenesis after fertilization under the control of nearby ICRs.[1,2]

As most imprinted genes have an important role in the growth and development of embryos, placental formation, and metabolism, aberrant expression of imprinted genes due to epigenetic or genetic abnormalities is often implicated in the pathogenesis of human disorders such as congenital anomalies and tumors.[1,2] Epigenetic abnormality leading to aberrant expression of imprinted genes mostly includes aberrant hypomethylation or hypermethylation at ICRs. Genetic abnormalities include uniparental disomies, chromosomal deletions, duplications, translocations, inversions of imprinting domains, and point mutations of imprinted genes. Representative imprinting disorders and their corresponding imprinted loci are as follows: Beckwith–Wiedemann syndrome (BWS) at 11p15.5, Prader-Willi/Angelman syndromes at 15q11-q13, pseudoparahypothyroidism type 1b at 20q13.3, Silver–Russell syndrome (SRS) at 11p15.5 and chromosome 7, and transient neonatal diabetes mellitus type 1 at 6q24.

Here, we review BWS, focusing especially on imprinting mechanisms of 11p15.5, epigenetic and genetic etiologies leading to

Division of Molecular Genetics and Epigenetics, Department of Biomolecular Sciences, Faculty of Medicine, Saga University, Saga, Japan
Correspondence: Professor H Soejima, Division of Molecular Genetics and Epigenetics, Department of Biomolecular Sciences, Faculty of Medicine, Saga University, 5-1-1 Nabeshima, Saga 849-8501, Japan.
E-mail: soejimah@cc.saga-u.ac.jp
Received 7 April 2013; revised 23 April 2013; accepted 26 April 2013; published online 30 May 2013

aberrant expression of corresponding imprinted genes, relationships between epigenetic/genetic alterations and clinical features, and associated childhood tumors. We also describe the relationship between assisted reproductive technology (ART) and imprinting disorders and explore multilocus hypomethylation disorders (MHDs).

CLINICAL FEATURES AND CAUSATIVE ALTERATIONS OF BWS

BWS (OMIM #130650) is a pediatric overgrowth disorder that is characterized by the peculiar traits of prenatal and postnatal macrosomia, macroglossia, abdominal wall defects as originally described by Beckwith and Wiedemann.[3,4] The incidence has been reported to be 1 in 13 700,[5] and the male-to-female ratio is ~1:1. BWS also shows other variable features, including anterior ear lobe creases and/or posterior helical pits, neonatal hypoglycemia, intra-abdominal visceromegaly, cytomegaly of adrenal fetal cortex, renal abnormalities, hemihyperplasia and cleft palate. The development of embryonal tumors (for example, Wilms' tumor, hepatoblastoma and rhabdomyosarcoma) is an important feature of BWS, and the overall tumor risk has been estimated at 7.5% with a range of 4–21%.[6,7] Although several clinical criteria have been proposed so far,[8–10] there is no single unified criterion. However, a criteria scheme proposed by Weksberg *et al.*[11] is generally accepted for clinical diagnosis: the presence of at least three major findings, or two major findings and one minor finding, from those reported in Table 1. Simpson–Golabi–Behmel syndrome, Costello syndrome, Perlman syndrome, Sotos syndrome and mucopolysaccharidosis VI (Maroteaux–Lamy syndrome) are considered as differential diagnoses.

Table 1 Major and minor finings associated with Beckwith–Wiedemann syndrome[11]

Major findings
Abdominal wall defect: omphalocele (exomphalos) or umbilical hernia
Macroglossia
Macrosomia (traditionally defined as height and weight >97th percentile)
Anterior ear lobe creases and/or posterior helical pits (bilateral or unilateral)
Visceromegaly of intra-abdominal organ(s); for example, liver kidney(s), spleen, pancreas and adrenal glands
Embryonal tumor in childhood
Hemihyperplasia
Cytomegaly of adrenal fetal cortex, usually diffuse and bilateral
Renal abnormalities, including medullary dysplasia and later development of Medullary sponge kidney
Positive family history of Beckwith–Wiedemann syndrome
Cleft palate
Minor findings
Pregnancy-related findings of polyhydramnios, enlarged placenta and/or thickened umbilical cord, premature onset of labor and delivery
Neonatal hypoglycemia
Nevus flammeus
Cardiomegaly/structural cardiac anomalies/cardiomyopathy
Diastasis recti
Advanced bone age

Approximately 85% of BWS cases are sporadic; the other 15% are familial showing autosomal dominant inheritance. The relevant imprinted chromosomal region in BWS, 11p15.5, consists of two independent imprinting domains, *IGF2/H19* and *CDKN1C/KCNQ1OT1*. Several causative alterations have been identified for sporadic cases of BWS: loss of methylation (LOM) at KvDMR1 (~50%), gain of methylation (GOM) at H19DMR (~5%), paternal uniparental disomy (patUPD; ~20%), *CDKN1C* mutations (~5%), duplications of 11p15 (<1%) and translocations or inversions involving 11p15 (<1%) (Table 2).[11–13] However, no alteration of 11p15.5 can be found for ~20% of BWS cases. Interestingly, among these causative alterations, methylation abnormalities, such as KvDMR1-LOM and H19DMR-GOM, and patUPD are mosaic in the patients; however, other genetic alterations including *CDKN1C* mutation are essentially not mosaic.

IMPRINTING MECHANISMS OF 11P15.5 AND ETIOLOGIES OF BWS

The *IGF2/H19* domain

The important genes in this domain are insulin-like growth factor 2 (*IGF2*) and *H19*. *IGF2* is expressed from the paternal allele, and the gene product has an important role in development and growth, whereas *H19* is a maternally-expressed, non-coding RNA, which may function as a tumor suppressor, but whose precise biological role remains unresolved.[14,15] One study reported that *H19* is a miRNA precursor expressed in human keratinocytes and neonatal mice, suggesting its involvement during development.[16] The ICR of this domain is H19DMR, which is located 2 kb upstream of *H19* and is methylated on the paternal but not the maternal allele (Figure 1). The methylation of H19DMR is established during spermatogenesis.[17,18] This ICR, which contains seven CCCTC-binding factor (CTCF) binding sites in human and four in mouse, regulates the reciprocal expression of *IGF2* and *H19* by functioning as a chromatin insulator. On the maternal allele, CTCF binding at the insulator elements within unmethylated H19DMR blocks enhancers downstream of *H19* from accessing *IGF2* promoters. On the paternal allele, as the methylation of H19DMR prevents CTCF binding, the enhancers can access *IGF2* promoters.[19,20] Thus, these mechanisms lead to paternal expression of *IGF2* and maternal expression of *H19*. Recent chromatin conformation studies showed that CTCF binding at regulatory regions other than H19DMR and the enhancers surrounding the domain formed allele-specific chromatin loops, depending on the methylation of H19DMR, in order to regulate the expression of *IGF2* and *H19*. For these CTCF-dependent chromatin loop formations, the recruitment of cohesin to CTCF-binding sites is required and cohesin stabilizes the chromatin conformations.[21,22]

Table 2 Correlation between epigenetic/genetic alteration and clinical features

Alteration type	*Frequency*	*Clinical features*	*Tumor risk*	*Tumor type*
H19DMR-GOM	2–7%	Hemihyperplasia	>25%	Wilms' tumor, Hepatoblastoma
KvDMR1-LOM	~50%	Omphalocele, Hemihyperplasia	~5%	Hepatoblastoma, Rhabdomyosarcoma, Gonadoblastoma (No Wilms' tumor)
Paternal uniparental disomy	~20%	Hemihyperplasia (various regions of body)	>25%	Wilms' tumor, Hepatoblastoma
CDKN1C mutation	~5%	Omphalocele, Cleft palate	<5%	Neuroblastoma
Chromosomal rearrangements	<2%	Developmental delay (case with duplication)	Unknown	Unknown

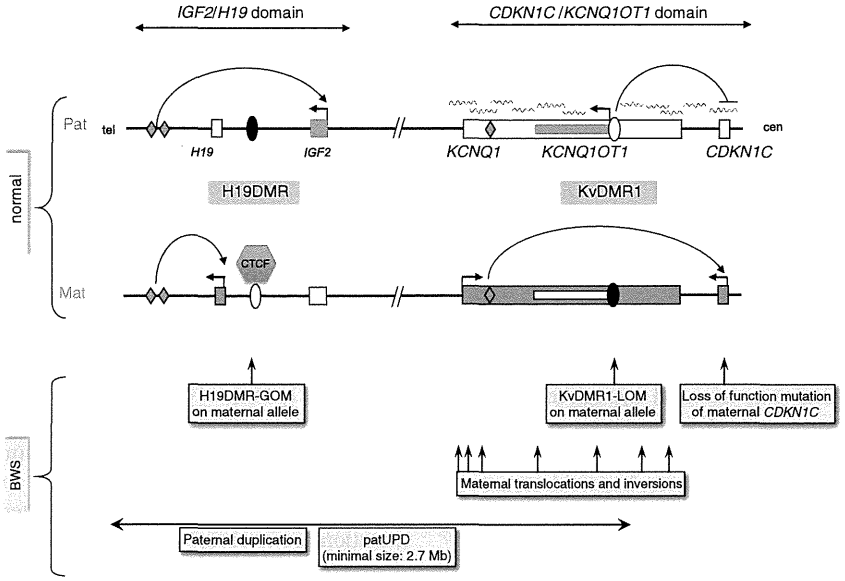

Figure 1 Imprinting domains at 11p15.5. Upper panel indicates the imprinting mechanisms in normal individuals. As for the *IGF2/H19* domain, the insulator model is shown. On the maternal chromosome, the binding of CTCF to unmethylated H19DMR blocks enhancers from accessing *IGF2* promoters. In contrast, on the paternal allele, as the methylation of H19DMR prevents CTCF binding, the enhancers can access *IGF2* promoters. Thus, these mechanisms lead to paternal expression of *IGF2* and maternal expression of *H19*. Please refer to the text for the chromatin loop model. As for the *CDKN1C/KCNQ1OT1* domain, on the paternal chromosome, it has been proposed that *CDKN1C* is repressed by *KCNQ1OT1* RNA coating and by a silencer and an insulator near the KvDMR1, which is likely regulated by CTCF. A putative enhancer within the *KCNQ1* locus acts on maternal expression of *CDKN1C*. The lower panel displays causative alterations of BWS. Vertical arrows with maternal translocations and inversions indicate chromosomal break points. Blue: paternal expressed genes; red: maternal expressed genes; green diamond: enhancers (putative enhancer in *CDKN1C/KCNQ1OT1* domain); wavy line: non-coding RNA transcribed from the paternal *KCNQ1OT1* gene.

In ~5% of BWS patients, gain of DNA methylation occurs on the normally unmethylated maternal H19DMR (H19DMR-GOM) (Figure 1, Table 2). Aberrant DNA methylation at maternal H19DMR is accompanied by a change of histone modification from accessible H3K9ac and bivalent H3K4me2/H3K27me3 to repressive H3K9me3 and H4K20me3.[22] The aberrant DNA methylation prevents CTCF binding to maternal H19DMR, and the chromatin loop formation changes from maternal-type to paternal-type due to aberrant DNA methylation and histone modification change. The chromatin conformation change drags the enhancers into the vicinity of *IGF2*, leading to biallelic expression and loss of imprinting of *IGF2* and reduced expression of *H19*. Overexpression of *IGF2* and reduced expression of *H19* induce the BWS phenotype. One representative phenotype of H19DMR-GOM is hemihyperplasia (Table 2).[12]

The majority of GOM cases show an isolated epigenetic alteration; however, ~20% of GOM cases are associated with genetic alterations, which are variable length microdeletions including CTCF-binding sites and point mutations and a deletion at the octamer-binding protein (OCT) binding site.[23] These genetic alterations lead to maternal H19DMR not being able to maintain an unmethylated status.[24,25] However, the mechanism by which isolated H19DMR-GOM occurs is still unknown. As a certain number of cases with isolated H19DMR-GOM show variable hypermethylation, patients have an epigenetic mosaic of normal cells and aberrantly methylated cells, indicating that GOM occurs in the post-fertilization stage, especially after implantation.[26–28]

Epimutation of H19DMR is also a cause of SRS (OMIM #180860), which is characterized by opposite clinical phenotypes such as growth restriction.[29] In ~40% of SRS patients, methylated paternal H19DMR becomes hypomethylated (H19DMR-LOM), leading to increased *H19* expression and decreased *IGF2* expression.[30] In contrast to BWS, essentially no mutations of H19DMR have been found in SRS patients with H19DMR-LOM. One SRS patient did exhibit a *de novo* mutation in H19DMR; however, as the mutation did not involve any putative protein-binding sites, it remains unknown if the mutation affected the methylation status of H19DMR.[23] As a majority of cases with H19DMR-LOM show variable hypermethylation, LOM also occurs in the post-fertilization stage.[29,31]

THE *CDKN1C/KCNQ1OT1* DOMAIN

The important genes in this domain are *CDKN1C* and *KCNQ1OT1*. *CDKN1C* encodes cyclin-dependent kinase inhibitor and shows preferential maternal expression. *KCNQ1OT1* is a paternally-expressed, long non-coding RNA. The ICR of this domain is KvDMR1, located in intron 10 of the *KCNQ1* gene, and it is methylated on the maternal but not the paternal allele (Figure 1). The methylation of KvDMR1 is established during oogenesis.[17,18] As KvDMR1 overlaps with the promoter of *KCNQ1OT1*, the paternal *KCNQ1OT1* is expressed from unmethylated paternal KvDMR1 in the opposite direction of *KCNQ1*, and it functions to silence genes in the domain *in cis*.[32] In mice, *Kcnq1ot1* RNA interacts with G9a and the PRC2 complex, which mediates repressive histone modifications such as H3K9me3 and H3K27me3, and forms a repressive nuclear compartment that leads to gene silencing within the domain, including of *Cdkn1c*. However, this mechanism is specific to the placenta.[33,34] In mouse liver, *Kcnq1ot1* RNA interacts with Dnmt1 to mediate maintenance of somatic DMRs, some of which overlap the *Cdkn1c* promoter, and silences genes within the domain.[35] In addition, the identification of paternal allele-specific CTCF binding to KvDMR1 suggests that a repressive element within KvDMR1 likely regulated by CTCF acts to silence paternal *Cdkn1c* specifically and without promoter methylation in a subset of tissues (for example,

kidney, liver and lung).[36,37] In humans, although *KCNQ1OT1* coats the neighboring regions of chromatin-containing *CDKN1C*, the *CDKN1C* promoter does not show DMR, and H3K9me may not be involved in *CDKN1C* repression.[38,39] In two BWS families with significantly reduced expression of *CDKN1C*, maternal microdeletions for most parts of the *KCNQ1* gene impact KvDMR1 and the following *KCNQ1OT1* gene, but not *CDKN1C*, suggesting the presence of an enhancer element within the *KCNQ1* locus for maternal expression of *CDKN1C*.[40,41] In addition, the DNA fragment containing KvDMR1 has been shown to have both silencer and insulator activities with CTCF binding.[42] Therefore, researchers have proposed that *CDKN1C* is repressed on the paternal chromosome by *KCNQ1OT1* RNA coating and by both a silencer and an insulator near KvDMR1, which is likely regulated by CTCF binding that prevents the *CDKN1C* promoter from accessing the enhancer downstream of KvDMR1.[41]

Loss of DNA methylation on the normally methylated maternal KvDMR1 (KvDMR1-LOM) accounts for ~50% of BWS patients (Figure 1, Table 2). KvDMR1-LOM is accompanied by loss of H3K9me2, and this leads to expression of *KCNQ1OT1* RNA, which in turn results in repression of *CDKN1C* expression on the maternal chromosome with the mechanism as proposed above.[39,41,43,44] In addition, only three families have been reported to have maternal transmission of the microdeletions containing KvDMR1, leading to reduced expression of *CDKN1C*.[40,41,45] Such reduced expression induces the BWS phenotype.

Representative phenotypes of KvDMR1-LOM include omphalocele and hemihyperplasia (Table 2).[12] As certain cases with isolated KvDMR1-LOM also display variable hypomethylation, patients are epigenetic mosaic, which indicates that LOM occurs in the post-fertilization stage.[46–49] Interestingly, monozygotic twins discordant for BWS are found predominantly for females. This could be in part explained by reduction of the amount of DNMT1 to maintain KvDMR1 methylation during the overlap in timing shared by X-inactivation and twinning.[46]

PATERNAL UNIPARENTAL DISOMY

patUPD of 11p is found in ~20% of patients (Figure 1, Table 2). All patients with patUPD are mosaic for patUPD cells and normal biparental cells, indicating occurrence of somatic recombination at the post-fertilization stage. Thus, UPD is always paternal isodisomy. Romanelli *et al.*[50] analyzed nine patients with patUPD using SNP arrays, and found that the minimal patUPD size was ~2.7 Mb from telomere to the centromeric side of KvDMR1 (Figure 1). As the minimal region includes both ICRs, H19DMR and KvDMR1, both H19DMR hypermethylation and KvDMR1 hypomethylation occur depending on the percentage of mosaicism and *IGF2* overexpression; reduced expression of *CDKN1C* must be induced. Meanwhile, Romanelli *et al.*[50] could not find hot-spots of mitotic recombination break points. One representative phenotypes of patUPD is hemihyperplasia, which can affect various regions of the body (Table 2).[12]

The largest patUPD size is the whole genome, denoted as genome-wide patUPD. Non-mosaic genome-wide patUPD results in hydatidiform mole formation. In contrast, individuals with mosaic genome-wide patUPD are born alive. To date, 11 patients with genome-wide patUPD have been reported.[51–58] Among these, half of the patients were diagnosed as BWS and only two displayed phenotypes associated with transient neonatal diabetes mellitus type 1 and upd(14)pat syndrome.[51,57] In addition, one patient with parthenogenic chimerism/mosaicism showed a SRS-like phenotype.[59] These findings suggested an epi-dominant effect of aberrant methylation of 11p15 on clinical features. However, genome-wide patUPD patients with BWS phenotypes display atypical and varied phenotypes. This would be attributable to a paternal epigenotype for all ICRs and being homozygous for mutations of autosomal recessive genes. In addition, patients exhibit a significantly increased predisposition for tumor development. This also would be attributable to inactivation of tumor suppressor genes, or activation of oncogenes.

CDKN1C MUTATION

As mentioned before, *CDKN1C* is a gene responsible for the pathogenesis of BWS within the *CDKN1C/KCNQ1OT1* domain, and it exhibits maternal preferential expression. This gene contains three exons divided by two introns encoding a 316 amino-acid protein, which is a strong inhibitor of several G1 cyclin/Cdk complexes and a negative regulator of cell proliferation.[60,61] The CDKN1C ($p57^{KIP2}$) protein consists of three distinct domains: a cyclin-dependent kinase inhibitory domain, a proline and alanine repeat domain, and a QT domain (Figure 2). The cyclin-dependent kinase inhibitory domain contains a cyclin-binding region, a cyclin-dependent kinase-binding region and a 3_{10} helix, which are both necessary and sufficient to bind and inhibit cyclin-dependent kinase activity.[60–62] Proline and alanine repeats interact with the LIM domain kinase 1 and regulate actin dynamics.[62–64] The QT domain contains a proliferating cell nuclear antigen (PCNA) binding domain, which can prevent DNA replication *in vitro* and S-phase entry *in vivo*, and a nuclear localization signal.[60,62,65]

The mutations are found in ~5% of sporadic cases, whereas dominant maternal transmission of germline mutations are found in 40% of familial BWS cases.[11,12] The mutations in sporadic cases should occur on the maternal allele because of maternal expression of *CDKN1C*. Approximately 30 mutations have been reported since the initial report by Hatada *et al.*[66–68] These mutations are either missense mutations localized to the cyclin-dependent kinase inhibitory domain or nonsense mutations, both of which result in loss of function and lead to the BWS phenotype (Figure 2). Representative phenotypes of *CDKN1C* mutations include omphalocele and cleft palate (Table 2).[12]

Recently, missense mutations in the PCNA binding domain have reported in the undergrowth developmental disorder IMAGe syndrome (OMIM #614732), which is characterized by intrauterine growth restriction, metaphyseal dysplasia, adrenal hypoplasia congenita, and genital anomalies (Figure 2).[69] Only maternal transmission of the mutation results in IMAGe syndrome, consistent with imprinting inheritance. Targeted expression of patient-associated mutations in *Drosophila* caused restricted eye and wing growth, suggesting a gain-of-function mechanism. The gain of function might be due to abolishment of PCNA dependent CDKN1C monoubiquitination.[69] It is intriguing that two opposite phenotypes, BWS and IMAGe syndrome, occur because of the mutations of the same *CDKN1C* gene. The biological role and molecular mechanism of the monoubiquitination should be elucidated to understand how the two disorders differ.

CHROMOSOMAL REARRANGEMENTS

Chromosomal rearrangements involving 11p—including duplications, balanced translocations and inversions—occur in <2% of BWS patients (Figure 1, Table 2). Paternal duplications of 11p15 result in BWS due to overexpression of *IGF2*,[70] whereas maternal duplications of 11p15 result in SRS.[71] SRS and BWS phenotypes associated with 11p duplications in a single family have been

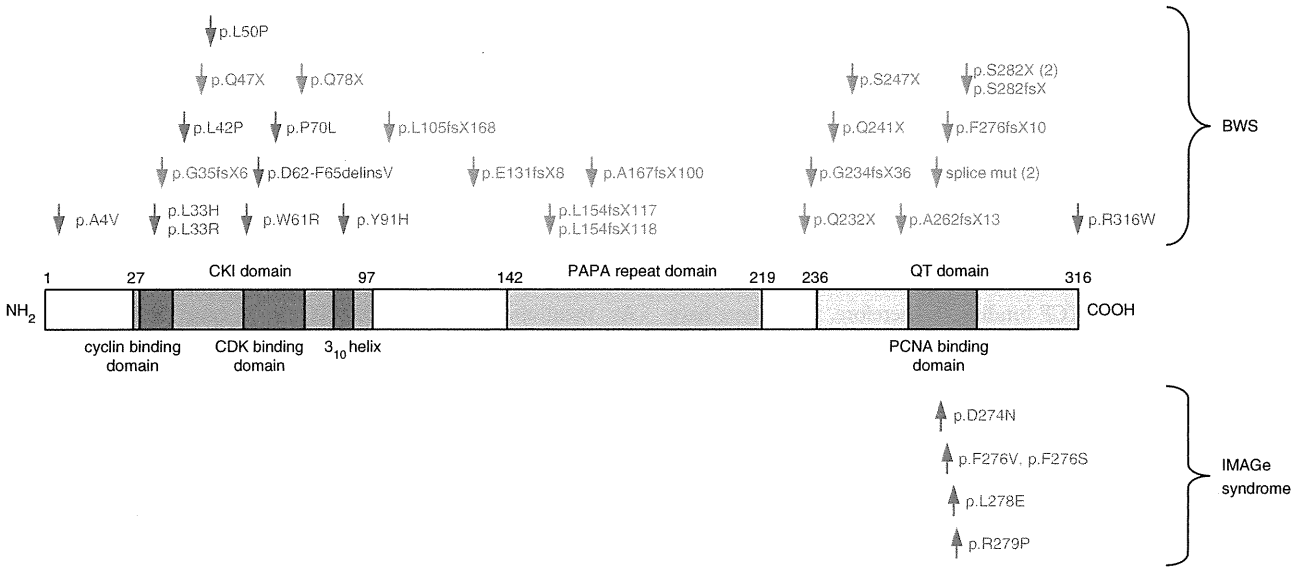

Figure 2 Mutations of *CDKN1C* in BWS and IMAGe syndrome.[67–69] The mutations in BWS are loss-of-function mutations, which are either amino-acid substitution mutations localized to the cyclin-dependent kinase inhibitory domain or truncating mutations. The mutations in IMAGe syndrome that lead to growth restriction are missense mutations specific to the PCNA-binding domain, considered a gain-of-function mutation. Blue: amino-acid substitution mutations; red: truncating mutations.

reported.[72] In this family, a SRS child was born from a mother with BWS phenotypes due to paternal duplication. Representative phenotypes of BWS due to duplication causes developmental delay (Table 2).[12]

So far at least 12 cases harboring translocations or inversions have been reported, with most break points of the translocations and inversions falling in the *KCNQ1* locus.[73–77] BWS develops when these are transmitted maternally. Three cases harboring inv(11)(p13;p15.5), inv(11)(p11.2;p15.5) and t(11;17)(p15.5;q21.3), respectively, have been seen to exhibit KvDMR1-LOM. However, a fibroblast with inv(11)(p15.5;q13) and a rhabdoid tumor line with t(11;22) have shown signs of reduced expression of *CDKN1C* with normal methylation at KvDMR1. These are consistent with the enhancer blocking insulator model mentioned before.[75–77] However, the remaining cases showed neither KvDMR1-LOM nor reduced expression of *CDKN1C*. Therefore, the developmental mechanism for BWS harboring translocations and inversions is largely unknown.

DIFFERENT RISKS FOR CHILDHOOD TUMORS IN EACH ALTERATION TYPE

Embryonal malignancies are the tumors most commonly associated with BWS—for example, Wilms' tumor, hepatoblastoma, adrenocortical carcinoma, rhabdomyosarcoma and neuroblastoma—but other malignant or benign tumors are occasionally observed.[6,7] Although overall tumor risk is ~7.5%, it is different for each causative alteration (Table 2). H19DMR-GOM and patUPD show the highest tumor risk, at >25%, especially for Wilms' tumor and hepatoblastoma. KvDMR1-LOM has a rate of developing hepatoblastoma, rhabdomyosarcoma and gonadoblastoma other than Wilms' tumors of ~5%.[10] The lowest risk is found in *CDKN1C* mutations with <5% of cases affected. Only neuroblastomas have been found in patients with *CDKN1C* mutations.[78,79] Wilms' tumors are frequently seen in patients with H19DMR-GOM or patUPD, but never seen in patients with KvDMR1-LOM or *CDKN1C* mutations, suggesting a critical role of *IGF2* overexpression in Wilms' tumor development. In fact, *IGF2* loss of imprinting is found in 60–70% of sporadic Wilms' tumors without 11p LOH.[80,81] Furthermore, *IGF2* loss of imprinting was also observed in ~21% of sporadic hepatoblastomas without 11p LOH, and aberrant methylations at H19DMR, H19 promoter, IGF2-DMR0 or IGF2-DMR2 were observed in ~55% of sporadic hepatoblastomas without 11p LOH, suggesting the importance of *IGF2* overexpression for hepatoblastoma development as well (Rumbajan JM *et al.*, submitted).[82] In addition, although many kinds of adult tumors display reduced *CDKN1C* expression, of which certain cases show KvDMR1-LOM, the risk of embryonal tumorigenesis is low in BWS patients with KvDMR1-LOM or *CDKN1C* mutations, suggesting different contributions of CDKN1C to tumor development between adulthood and childhood.

ART AND BWS

The worldwide usage of ART has increased. Several reports have raised concerns that the risk of imprinting disorders, such as BWS and Angelman syndrome, are increased in children conceived by ART, especially through *in vitro* fertilization and intracytoplasmic sperm injection, as the first reported associations in 2002 and 2003 between Angelman syndrome and BWS, respectively, with ART.[83–85] The risk of BWS is estimated to be six to nine times higher in children conceived by ART than in children conceived naturally.[86] The causative alteration for most of ART-related BWS is KvDMR1-LOM. The cause of Angelman syndrome is also LOM at *SNRPN*.

Animal studies have suggested that ovarian stimulation and culture medium for the embryo can affect DNA methylation and the expression of several imprinted genes.[87–90] In fact, 'large offspring syndrome' has been described as caused by LOM of the maternal *Igf2r* after sheep embryo culture.[91] However, in humans, although ovarian stimulation may predispose to aberrant methylation at imprinted loci,[92] it is still unclear whether the procedure of ART affects methylation at imprinted loci because ART populations are different from naturally conceived populations having low fertility rates, increased frequency of reproductive loss and advanced age.[93] Indeed, male infertility is strongly associated with aberrant methylation at both maternal and paternal alleles.[94,95] It has been

reported that there are no phenotypic differences between ART-related BWS and naturally conceived BWS.[96] However, Lim *et al.*[97] provided evidence that ART-related BWS had a significantly lower frequency of exomphalos and higher risk of tumor development than Wilms' tumor. Larger size studies are needed to better understand the correlation between ART and BWS.

MULTILOCUS HYPOMETHYLATION DISORDERS

Hypomethylations at several other imprinted loci have been reported to occur in BWS patients with KvDMR1-LOM.[47–49,97] As this phenomenon was also seen in patients with transient neonatal diabetes mellitus type 1 and SRS, a new entity of imprinting disorders such as MHD has been proposed.[49,98–101] The literature indicates an overall frequency of multilocus hypomethylation in BWS patients with KvDMR1-LOM of 20% (49/244).[49,98–101] *IGF2R-DMR2*, *GNAS*, *NESPAS*, *PEG1* and *PLAGL1* are frequently hypomethylated DMRs. In BWS patients, only maternally methylated DMRs displayed hypomethylation; however, several SRS patients with H19DMR-LOM showed hypomethylation at *DLK1/GTL2* IG-DMR, another paternally methylated DMR, indicating involvement of both maternally and paternally methylated DMRs. In addition, a certain SRS showed hypomethylation at both H19DMR and KvDMR1.[48,100] As these hypomethylations were mosaic, they were presumed to be due to a post-fertilization event.

Lim *et al.*[97] reported that ART-related BWS show multilocus hypomethylation more frequently than naturally conceived BWS; however, no such difference was observed by Rossignol *et al.*[47] One study reported that BWS with multilocus hypomethylation displayed characteristics not usually associated with BWS, such as speech retardation, peri/postnatal apnea, feeding difficulties and hearing problems; additionally, nevus flammeus and hemihypertrophy were significantly lower in patients with multilocus hypomethylation.[49] However, three other studies reported no difference in clinical features between MHDs and monolocus hypomethylation disorders.[47,48,97] As the studies so far have analyzed only limited numbers of DMRs, further investigation of all known DMRs are needed.

The involvement of trans-acting factors in these MHD has been suggested. In fact, in one study, homozygous and compound heterozygous mutations of *ZFP57*, which encodes a KRAB zinc-finger protein and is required for the post-fertilization maintenance of maternal and paternal methylation imprinting at multiple loci, were found in transient neonatal diabetes mellitus type 1 patients with multilocus hypomethylation.[102] However, no mutations were found in 27 BWS patients with KvDMR1-LOM probably without multilocus hypomethylation.[103] KAP1, a protein associated with ZFP57, interacts with DNMT1 and binds to many ICRs in embryonic stem cells to maintain DNA and histone methylation.[104,105] Mice with maternal deletions of *Trim28*, a homolog of human *KAP1*, show aberrant DNA demethylation at a few ICRs.[106] Mutation searches of *KAP1* in MHD patients have not been reported to date.

Other candidates for trans-acting factors are NLRP2 and NLRP7, which are members of the Nod-like receptor protein (NLRP) family. Some NLRPs are components of the inflammasome, an assembly that is implicated in the sensing of, and inflammatory reaction to, extracellular pathogens and intracellular noxious compounds.[107] Mutations of *NLRP2* were identified in a familial case of BWS with KvDMR1-LOM and PEG1-LOM, suggesting a role of NLRP2 in the establishment or maintenance of ICRs.[108] However, the mutation has not been corroborated by other studies yet. Mutations of *NLRP7* and *C6ORF221* account for familial biparental hydatidiform mole, which is a maternal effect recessive disorder resulting from failure of maternal imprints.[109,110] Mutation searches of *NLRP7* were performed on the mother of a patient showing both transient neonatal diabetes mellitus type 1 and BWS features with multilocus hypomethylation, but they were unsuccessful.[99] In addition, DNMT3L, which is required for establishing maternal imprints, was not mutated in two BWS patients with severe multilocus hypomethylation.[49] Mutation searching of all candidate trans-acting factors should be performed over a large number of MHD patients to explore this matter further.

In addition, one circular chromosome conformation capture (4C) study revealed that maternal H19DMR interacts with the autosomal region, and imprinting domains were strongly overrepresented in the 4C library, suggesting the involvement of higher order chromatin interaction in the regulation of imprinting.[111] The involvement of physical chromosome interactions in MHD should also be further elucidated.

CONCLUSIONS

Although H19DMR-GOM, KvDMR1-LOM, patUPD and *CDKN1C* mutations, and chromosomal rearrangements account for ~80% of BWS phenotypes, several questions about these alterations still remain to be clarified. In addition, at least 20% of patients do not have these associated alterations, suggesting the existence of other, unknown epigenetic/genetic defects. Furthermore, other issues, such as the effect of ART on imprinting disorders and the mechanism of multilocus imprinting establishment/maintenance, should be clarified. Further investigations of all of these issues must be elucidated in order to understand the molecular basis of BWS and related imprinting disorders.

ACKNOWLEDGEMENTS

This study was supported, in part, by a Grant for Research on Intractable Diseases from the Ministry of Health, Labor, and Welfare; a Grant for Child Health and Development from the National Center for Child Health and Development; a Grant-in-Aid for Challenging Exploratory Research; and, a Grant-in-Aid for Young Scientists (B) from the Japan Society for the Promotion of Science.

1 Abramowitz, L. K. & Bartolomei, M. S. Genomic imprinting: recognition and marking of imprinted loci. *Curr. Opin. Genet. Dev.* **22,** 72–78 (2012).
2 Tomizawa, S. & Sasaki, H. Genomic imprinting and its relevance to congenital disease, infertility, molar pregnancy and induced pluripotent stem cell. *J. Hum. Genet.* **57,** 84–91 (2012).
3 Beckwith, JB. Extreme cytomegaly of the adrenal fetal cortex, omphalocele, hyperplasia of kidneys and pancreas, and Leydig-cell hyperplasia: Another syndrome? Abstract, Western Society for Pediatric Research, Los Angeles, CA (1963).
4 Wiedemann, H. Complexe malformatif familial avec hernie ombilicale et macroglossia, un syndrome nouveau. *J. Genet. Hum.* **13,** 223–232 (1964).
5 Thorburn, M. J., Wright, E. S., Miller, C. G. & Smith-Read, E. H. Exomphalos-macroglossia-gigantism syndrome in Jamaican infants. *Am J Dis Child* **119,** 316–321 (1970).
6 Rump, P., Zeegers, M. P. & van Essen, A. J. Tumor risk in Beckwith-Wiedemann syndrome: a review and meta-analysis. *Am. J. Med. Genet. A.* **136,** 95–104 (2005).
7 Lapunzina, P. Risk of tumorigenesis in overgrowth syndromes: a comprehensive review. *Am. J. Med. Genet. C. Semin. Med. Genet.* **137C,** 53–71 (2005).
8 Elliott, M., Bayly, R., Cole, T., Temple, I. K. & Maher, E. R. Clinical features and natural history of Beckwith-Wiedemann syndrome: presentation of 74 new cases. *Clin. Genet.* **46,** 168–174 (1994).
9 DeBaun, M. R. & Tucker, M. A. Risk of cancer during the first four years of life in children from The Beckwith-Wiedemann Syndrome Registry. *J. Pediatr.* **132,** 398–400 (1998).
10 Weksberg, R., Nishikawa, J., Caluseriu, O., Fei, Y. L., Shuman, C., Wei, C. *et al.* Tumor development in the Beckwith-Wiedemann syndrome is associated with a variety of constitutional molecular 11p15 alterations including imprinting defects of KCNQ1OT1. *Hum. Mol. Genet.* **10,** 2989–3000 (2001).

11 Weksberg, R., Shuman, C. & Beckwith, J. B. Beckwith-Wiedemann syndrome. *Eur. J. Hum. Genet.* **18,** 8–14 (2010).
12 Choufani, S., Shuman, C. & Weksberg, R. Beckwith-Wiedemann syndrome. *Am. J. Med. Genet. C. Semin. Med. Genet.* **154C,** 343–354 (2010).
13 Sasaki, K., Soejima, H., Higashimoto, K., Yatsuki, H., Ohashi, H., Yakabe, S. *et al.* Japanese and North American/European patients with Beckwith-Wiedemann syndrome have different frequencies of some epigenetic and genetic alterations. *Eur. J. Hum. Genet.* **15,** 1205–1210 (2007).
14 Hao, Y., Crenshaw, T., Moulton, T., Newcomb, E. & Tycko, B. Tumour-suppressor activity of H19 RNA. *Nature* **365,** 764–767 (1993).
15 Onyango, P. & Feinberg, A. P. A nucleolar protein, H19 opposite tumor suppressor (HOTS), is a tumor growth inhibitor encoded by a human imprinted H19 antisense transcript. *Proc. Natl Acad. Sci. USA* **108,** 16759–16764 (2011).
16 Cai, X. & Cullen, B. R. The imprinted H19 noncoding RNA is a primary microRNA precursor. *RNA* **13,** 313–316 (2007).
17 Li, E. Chromatin modification and epigenetic reprogramming in mammalian development. *Nat. Rev. Genet.* **3,** 662–673 (2002).
18 Sasaki, H. & Matsui, Y. Epigenetic events in mammalian germ-cell development: reprogramming and beyond. *Nat. Rev. Genet.* **9,** 129–140 (2008).
19 Bell, A. C. & Felsenfeld, G. Methylation of a CTCF-dependent boundary controls imprinted expression of the Igf2 gene. *Nature* **405,** 482–485 (2000).
20 Hark, A. T., Schoenherr, C. J., Katz, D. J., Ingram, R. S., Levorse, J. M. & Tilghman, S. M. CTCF mediates methylation-sensitive enhancer-blocking activity at the H19/Igf2 locus. *Nature* **405,** 486–489 (2000).
21 Nativio, R., Wendt, K. S., Ito, Y., Huddleston, J. E., Uribe-Lewis, S., Woodfine, K. *et al.* Cohesin is required for higher-order chromatin conformation at the imprinted IGF2-H19 locus. *PLoS Genet.* **5,** e1000739 (2009).
22 Nativio, R., Sparago, A., Ito, Y., Weksberg, R., Riccio, A. & Murrell, A. Disruption of genomic neighbourhood at the imprinted IGF2-H19 locus in Beckwith-Wiedemann syndrome and Silver-Russell syndrome. *Hum. Mol. Genet.* **20,** 1363–1374 (2011).
23 Demars, J., Shmela, M. E., Rossignol, S., Okabe, J., Netchine, I., Azzi, S. *et al.* Analysis of the IGF2/H19 imprinting control region uncovers new genetic defects, including mutations of OCT-binding sequences, in patients with 11p15 fetal growth disorders. *Hum. Mol. Genet.* **19,** 803–814 (2010).
24 Hori, N., Nakano, H., Takeuchi, T., Kato, H., Hamaguchi, S., Oshimura, M. *et al.* A dyad oct-binding sequence functions as a maintenance sequence for the unmethylated state within the H19/Igf2-imprinted control region. *J. Biol. Chem.* **277,** 27960–27967 (2002).
25 Fedoriw, A. M., Stein, P., Svoboda, P., Schultz, R. M. & Bartolomei, M. S. Transgenic RNAi reveals essential function for CTCF in H19 gene imprinting. *Science* **303,** 238–240 (2004).
26 Sparago, A., Russo, S., Cerrato, F., Ferraiuolo, S., Castorina, P., Selicorni, A. *et al.* Mechanisms causing imprinting defects in familial Beckwith-Wiedemann syndrome with Wilms' tumour. *Hum. Mol. Genet.* **16,** 254–264 (2007).
27 Cerrato, F., Sparago, A., Verde, G., De Crescenzo, A., Citro, V., Cubellis, M. V. *et al.* Different mechanisms cause imprinting defects at the IGF2/H19 locus in Beckwith-Wiedemann syndrome and Wilms' tumour. *Hum. Mol. Genet.* **17,** 1427–1435 (2008).
28 Higashimoto, K., Nakabayashi, K., Yatsuki, H., Yoshinaga, H., Jozaki, K., Okada, J. *et al.* Aberrant methylation of H19-DMR acquired after implantation was dissimilar in soma versus placenta of patients with Beckwith-Wiedemann syndrome. *Am. J. Med. Genet. A.* **158A,** 1670–1675 (2012).
29 Gicquel, C., Rossignol, S., Cabrol, S., Houang, M., Steunou, V., Barbu, V. *et al.* Epimutation of the telomeric imprinting center region on chromosome 11p15 in Silver-Russell syndrome. *Nat Genet.* **37,** 1003–1007 (2005).
30 Eggermann, T., Begemann, M., Binder, G. & Spengler, S. Silver-Russell syndrome: genetic basis and molecular genetic testing. *Orphanet. J. Rare Dis.* **5,** 19 (2010).
31 Bliek, J., Terhal, P., van den Bogaard, M. J., Maas, S., Hamel, B., Salieb-Beugelaar, G. *et al.* Hypomethylation of the H19 gene causes not only Silver-Russell syndrome (SRS) but also isolated asymmetry or an SRS-like phenotype. *Am. J. Hum. Genet.* **78,** 604–614 (2006).
32 Mancini-Dinardo, D., Steele, S. J., Levorse, J. M., Ingram, R. S. & Tilghman, S. M. Elongation of the Kcnq1ot1 transcript is required for genomic imprinting of neighboring genes. *Genes Dev.* **20,** 1268–1282 (2006).
33 Pandey, R. R., Mondal, T., Mohammad, F., Enroth, S., Redrup, L., Komorowski, J. *et al.* Kcnq1ot1 antisense noncoding RNA mediates lineage-specific transcriptional silencing through chromatin-level regulation. *Mol. Cell.* **32,** 232–246 (2008).
34 Terranova, R., Yokobayashi, S., Stadler, M. B., Otte, A. P., van Lohuizen, M., Orkin, S. H. *et al.* Polycomb group proteins Ezh2 and Rnf2 direct genomic contraction and imprinted repression in early mouse embryos. *Dev. Cell.* **15,** 668–679 (2008).
35 Mohammad, F., Mondal, T., Guseva, N., Pandey, G. K. & Kanduri, C. Kcnq1ot1 noncoding RNA mediates transcriptional gene silencing by interacting with Dnmt1. *Development* **137,** 2493–2499 (2010).
36 Fitzpatrick, G. V., Pugacheva, E. M., Shin, J. Y., Abdullaev, Z., Yang, Y., Khatod, K. *et al.* Allele-specific binding of CTCF to the multipartite imprinting control region KvDMR1. *Mol. Cell. Biol.* **27,** 2636–2647 (2007).
37 Shin, J. Y., Fitzpatrick, G. V. & Higgins, M. J. Two distinct mechanisms of silencing by the KvDMR1 imprinting control region. *EMBO J.* **27,** 168–178 (2008).
38 Murakami, K., Oshimura, M. & Kugoh, H. Suggestive evidence for chromosomal localization of non-coding RNA from imprinted LIT1. *J. Hum. Genet.* **52,** 926–933 (2007).
39 Soejima, H., Nakagawachi, T., Zhao, W., Higashimoto, K., Urano, T., Matsukura, S. *et al.* Silencing of imprinted CDKN1C gene expression is associated with loss of CpG and histone H3 lysine 9 methylation at DMR-LIT1 in esophageal cancer. *Oncogene* **23,** 4380–4388 (2004).
40 Niemitz, E. L., DeBaun, M. R., Fallon, J., Murakami, K., Kugoh, H., Oshimura, M. *et al.* Microdeletion of LIT1 in familial Beckwith-Wiedemann syndrome. *Am. J. Hum. Genet.* **75,** 844–849 (2004).
41 Algar, E., Dagar, V., Sebaj, M. & Pachter, N. An 11p15 imprinting centre region 2 deletion in a family with Beckwith Wiedemann syndrome provides insights into imprinting control at CDKN1C. *PLoS One* **6,** e29034 (2011).
42 Du, M., Beatty, L. G., Zhou, W., Lew, J., Schoenherr, C., Weksberg, R. *et al.* Insulator and silencer sequences in the imprinted region of human chromosome 11p15.5. *Hum. Mol. Genet.* **12,** 1927–1939 (2003).
43 Higashimoto, K., Urano, T., Sugiura, K., Yatsuki, H., Joh, K., Zhao, W. *et al.* Loss of CpG methylation is strongly correlated with loss of histone H3 lysine 9 methylation at DMR-LIT1 in patients with Beckwith-Wiedemann syndrome. *Am. J. Hum. Genet.* **73,** 948–956 (2003).
44 Diaz-Meyer, N., Day, C. D., Khatod, K., Maher, E. R., Cooper, W., Reik, W. *et al.* Silencing of CDKN1C (p57KIP2) is associated with hypomethylation at KvDMR1 in Beckwith-Wiedemann syndrome. *J. Med. Genet.* **40,** 797–801 (2003).
45 Zollino, M., Orteschi, D., Marangi, G., De Crescenzo, A., Pecile, V., Riccio, A. *et al.* A case of Beckwith-Wiedemann syndrome caused by a cryptic 11p15 deletion encompassing the centromeric imprinted domain of the BWS locus. *J. Med. Genet.* **47,** 429–432 (2010).
46 Weksberg, R., Shuman, C., Caluseriu, O., Smith, A. C., Fei, Y. L., Nishikawa, J. *et al.* Discordant KCNQ1OT1 imprinting in sets of monozygotic twins discordant for Beckwith-Wiedemann syndrome. *Hum. Mol. Genet.* **11,** 1317–1325 (2002).
47 Rossignol, S., Steunou, V., Chalas, C., Kerjean, A., Rigolet, M., Viegas-Pequignot, E. *et al.* The epigenetic imprinting defect of patients with Beckwith-Wiedemann syndrome born after assisted reproductive technology is not restricted to the 11p15 region. *J. Med. Genet.* **43,** 902–907 (2006).
48 Azzi, S., Rossignol, S., Steunou, V., Sas, T., Thibaud, N., Danton, F. *et al.* Multilocus methylation analysis in a large cohort of 11p15-related foetal growth disorders (Russell Silver and Beckwith Wiedemann syndromes) reveals simultaneous loss of methylation at paternal and maternal imprinted loci. *Hum. Mol. Genet.* **18,** 4724–4733 (2009).
49 Bliek, J., Verde, G., Callaway, J., Maas, S. M., De Crescenzo, A., Sparago, A. *et al.* Hypomethylation at multiple maternally methylated imprinted regions including PLAGL1 and GNAS loci in Beckwith-Wiedemann syndrome. *Eur. J. Hum. Genet.* **17,** 611–619 (2009).
50 Romanelli, V., Meneses, H. N., Fernández, L., Martínez-Glez, V., Gracia-Bouthelier, R., F Fraga, M. *et al.* Beckwith-Wiedemann syndrome and uniparental disomy 11p: fine mapping of the recombination breakpoints and evaluation of several techniques. *Eur. J. Hum. Genet.* **19,** 416–421 (2011).
51 Bryke, C., Garber, A. & Israel, J. Evolution of a complex phenotype in a unique patient with a paternal uniparental disomy for every chromosome cell line and a normal biparental inheritance cell line. Abstract, The annual meeting of The American Society of Human Genetics, Toronto, Canada (2004).
52 Giurgea, I., Sanlaville, D., Fournet, J. C., Sempoux, C., Bellanné-Chantelot, C., Touati, G. *et al.* Congenital hyperinsulinism and mosaic abnormalities of the ploidy. *J. Med. Genet.* **43,** 248–254 (2006).
53 Hoban, P. R., Heighway, J., White, G. R., Baker, B., Gardner, J., Birch, J. M. *et al.* Genome-wide loss of maternal alleles in a nephrogenic rest and Wilms' tumour from a BWS patient. *Hum. Genet.* **95,** 651–656 (1995).
54 Reed, R. C., Beischel, L., Schoof, J., Johnson, J., Raff, M. L. & Kapur, R. P. Androgenetic/biparental mosaicism in an infant with hepatic mesenchymal hamartoma and placental mesenchymal dysplasia. *Pediatr. Dev. Pathol.* **11,** 377–383 (2008).
55 Romanelli, V., Nevado, J., Fraga, M., Trujillo, A. M., Mori, M., Fernández, L. *et al.* Constitutional mosaic genome-wide uniparental disomy due to diploidisation: an unusual cancer-predisposing mechanism. *J. Med. Genet.* **48,** 212–216 (2011).
56 Wilson, M., Peters, G., Bennetts, B., McGillivray, G., Wu, Z. H., Poon, C. *et al.* The clinical phenotype of mosaicism for genome-wide paternal uniparental disomy: two new reports. *Am. J. Med. Genet. A.* **146A,** 137–148 (2008).
57 Yamazawa, K., Nakabayashi, K., Matsuoka, K., Masubara, K., Hata, K., Horikawa, R. *et al.* Androgenetic/biparental mosaicism in a girl with Beckwith-Wiedemann syndrome-like and upd(14)pat-like phenotypes. *J. Hum. Genet.* **56,** 91–93 (2011).
58 Inbar-Feigenberg, M., Choufani, S., Cytrynbaum, C., Chen, Y. A., Steele, L., Shuman, C. *et al.* Mosaicism for genome-wide paternal uniparental disomy with features of multiple imprinting disorders: diagnostic and management issues. *Am. J. Med. Genet. A.* **161A,** 13–20 (2013).
59 Yamazawa, K., Nakabayashi, K., Kagami, M., Sato, T., Saitoh, S., Horikawa, R. *et al.* Parthenogenetic chimaerism/mosaicism with a Silver-Russell syndrome-like phenotype. *J. Med. Genet.* **47,** 782–785 (2010).
60 Lee, M. H., Reynisdóttir, I. & Massagué, J. Cloning of p57KIP2, a cyclin-dependent kinase inhibitor with unique domain structure and tissue distribution. *Genes. Dev.* **9,** 639–649 (1995).
61 Matsuoka, S., Edwards, M. C., Bai, C., Parker, S., Zhang, P., Baldini, A. *et al.* p57KIP2, a structurally distinct member of the p21CIP1 Cdk inhibitor family, is a candidate tumor suppressor gene. *Genes Dev.* **9,** 650–662 (1995).
62 Borriello, A., Caldarelli, I., Bencivenga, D., Criscuolo, M., Cucciolla, V., Tramontano, A. *et al.* p57(Kip2) and cancer: time for a critical appraisal. *Mol. Cancer Res.* **9,** 1269–1284 (2011).

63 Yokoo, T., Toyoshima, H., Miura, M., Wang, Y., Iida, K. T., Suzuki, H. *et al.* p57Kip2 regulates actin dynamics by binding and translocating LIM-kinase 1 to the nucleus. *J. Biol. Chem.* **278,** 52919–52923 (2003).
64 Vlachos, P. & Joseph, B. The Cdk inhibitor p57(Kip2) controls LIM-kinase 1 activity and regulates actin cytoskeleton dynamics. *Oncogene* **28,** 4175–4188 (2009).
65 Watanabe, H., Pan, Z. Q., Schreiber-Agus, N., DePinho, R. A., Hurwitz, J. & Xiong, Y. Suppression of cell transformation by the cyclin-dependent kinase inhibitor p57KIP2 requires binding to proliferating cell nuclear antigen. *Proc. Natl Acad. Sci. USA* **95,** 1392–1397 (1998).
66 Hatada, I., Ohashi, H., Fukushima, Y., Kaneko, Y., Inoue, M., Komoto, Y. *et al.* An imprinted gene p57KIP2 is mutated in Beckwith-Wiedemann syndrome. *Nat. Genet.* **14,** 171–173 (1996).
67 Romanelli, V., Belinchón, A., Benito-Sanz, S., Martínez-Glez, V., Gracia-Bouthelier, R., Heath, K. E. *et al.* CDKN1C (p57(Kip2)) analysis in Beckwith-Wiedemann syndrome (BWS) patients: Genotype-phenotype correlations, novel mutations, and polymorphisms. *Am. J. Med. Genet. A.* **152A,** 1390–1397 (2010).
68 Yatsuki, H., Higashimoto, K., Jozaki, K., Koide, K., Okada, J., Watanabe, Y. *et al.* Novel mutations of CDKN1C in Japanese patients with Beckwith-Wiedemann syndrome. *Genes Genom* **35,** 141–147 (2013).
69 Arboleda, V. A., Lee, H., Parnaik, R., Fleming, A., Banerjee, A., Ferraz-de-Souza, B. *et al.* Mutations in the PCNA-binding domain of CDKN1C cause IMAGe syndrome. *Nat. Genet.* **44,** 788–792 (2012).
70 Waziri, M., Patil, S. R., Hanson, J. W. & Bartley, J. A. Abnormality of chromosome 11 in patients with features of Beckwith-Wiedemann syndrome. *J. Pediatr.* **102,** 873–876 (1983).
71 Eggermann, T., Spengler, S., Bachmann, N., Baudis, M., Mau-Holzmann, U. A., Singer, S. *et al.* Chromosome 11p15 duplication in Silver-Russell syndrome due to a maternally inherited translocation t(11;15). *Am. J. Med. Genet. A.* **152A,** 1484–1487 (2010).
72 Cardarelli, L., Sparago, A., De Crescenzo, A., Nalesso, E., Zavan, B., Cubellis, M. V. *et al.* Silver-Russell syndrome and Beckwith-Wiedemann syndrome phenotypes associated with 11p duplication in a single family. *Pediatr. Dev. Pathol.* **13,** 326–330 (2010).
73 Hoovers, J. M., Kalikin, L. M., Johnson, L. A., Alders, M., Redeker, B., Law, D. J. *et al.* Multiple genetic loci within 11p15 defined by Beckwith-Wiedemann syndrome rearrangement breakpoints and subchromosomal transferable fragments. *Proc. Natl Acad. Sci. USA* **92,** 12456–12460 (1995).
74 Lee, M. P., Hu, R. J., Johnson, L. A. & Feinberg, A. P. Human KVLQT1 gene shows tissue-specific imprinting and encompasses Beckwith-Wiedemann syndrome chromosomal rearrangements. *Nat. Genet.* **15,** 181–185 (1997).
75 Smilinich, N. J., Day, C. D., Fitzpatrick, G. V., Caldwell, G. M., Lossie, A. C., Cooper, P. R. *et al.* A maternally methylated CpG island in KvLQT1 is associated with an antisense paternal transcript and loss of imprinting in Beckwith-Wiedemann syndrome. *Proc. Natl Acad. Sci. USA* **96,** 8064–8069 (1999).
76 Kaltenbach, S., Capri, Y., Rossignol, S., Denjoy, I., Soudée, S., Aboura, A. *et al.* Beckwith-Wiedemann syndrome and long QT syndrome due to familial-balanced translocation t(11;17)(p15.5;q21.3) involving the KCNQ1 gene. *Clin. Genet.* (e-pub ahead of print 15 October 2012; doi:10.1111/cge.12038).
77 Smith, A. C., Suzuki, M., Thompson, R., Choufani, S., Higgins, M. J., Chiu, I. W. *et al.* Maternal gametic transmission of translocations or inversions of human chromosome 11p15.5 results in regional DNA hypermethylation and downregulation of CDKN1C expression. *Genomics* **99,** 25–35 (2012).
78 Lee, M. P., DeBaun, M., Randhawa, G., Reichard, B. A., Elledge, S. J. & Feinberg, A. P. Low frequency of p57KIP2 mutation in Beckwith-Wiedemann syndrome. *Am. J. Hum. Genet.* **61,** 304–309 (1997).
79 Gaston, V., Le Bouc, Y., Soupre, V., Burglen, L., Donadieu, J., Oro, H. *et al.* Analysis of the methylation status of the KCNQ1OT and H19 genes in leukocyte DNA for the diagnosis and prognosis of Beckwith-Wiedemann syndrome. *Eur. J. Hum. Genet.* **9,** 409–418 (2001).
80 Mummert, S. K., Lobanenkov, V. A. & Feinberg, A. P. Association of chromosome arm 16q loss with loss of imprinting of insulin-like growth factor-II in Wilms tumor. *Genes. Chromosomes. Cancer* **43,** 155–161 (2005).
81 Satoh, Y., Nakadate, H., Nakagawachi, T., Higashimoto, K., Joh, K., Masaki, Z. *et al.* Genetic and epigenetic alterations on the short arm of chromosome 11 are involved in a majority of sporadic Wilms' tumours. *Br. J. Cancer* **95,** 541–547 (2006).
82 Honda, S., Arai, Y., Haruta, M., Sasaki, F., Ohira, M., Yamaoka, H. *et al.* Loss of imprinting of IGF2 correlates with hypermethylation of the H19 differentially methylated region in hepatoblastoma. *Br J Cancer* **99,** 1891–1899 (2008).
83 Cox, G. F., Bürger, J., Lip, V., Mau, U. A., Sperling, K., Wu, B. L. *et al.* Intracytoplasmic sperm injection may increase the risk of imprinting defects. *Am. J. Hum. Genet.* **71,** 162–164 (2002).
84 DeBaun, M. R., Niemitz, E. L. & Feinberg, A. P. Association of *in vitro* fertilization with Beckwith-Wiedemann syndrome and epigenetic alterations of LIT1 and H19. *Am. J. Hum. Genet.* **72,** 156–160 (2003).
85 Gicquel, C., Gaston, V., Mandelbaum, J., Siffroi, J. P., Flahault, A. & Le Bouc, Y. *In vitro* fertilization may increase the risk of Beckwith-Wiedemann syndrome related to the abnormal imprinting of the KCN1OT gene. *Am. J. Hum. Genet.* **72,** 1338–1341 (2003).
86 Manipalviratn, S., DeCherney, A. & Segars, J. Imprinting disorders and assisted reproductive technology. *Fertil. Steril.* **91,** 305–315 (2009).
87 Doherty, A. S., Mann, M. R., Tremblay, K. D., Bartolomei, M. S. & Schultz, R. M. Differential effects of culture on imprinted H19 expression in the preimplantation mouse embryo. *Biol. Reprod.* **62,** 1526–1535 (2000).
88 Fauque, P., Jouannet, P., Lesaffre, C., Ripoche, M. A., Dandolo, L., Vaiman, D. *et al.* Assisted reproductive technology affects developmental kinetics, H19 Imprinting control region methylation and H19 gene expression in individual mouse embryos. *BMC Dev. Biol.* **7,** 116 (2007).
89 Zaitseva, I., Zaitsev, S., Alenina, N., Bader, M. & Krivokharchenko, A. Dynamics of DNA-demethylation in early mouse and rat embryos developed *in vivo* and *in vitro*. *Mol. Reprod. Dev.* **74,** 1255–1261 (2007).
90 Rivera, R. M., Stein, P., Weaver, J. R., Mager, J., Schultz, R. M. & Bartolomei, M. S. Manipulations of mouse embryos prior to implantation result in aberrant expression of imprinted genes on day 9.5 of development. *Hum. Mol. Genet.* **17,** 1–14 (2008).
91 Young, L. E., Fernandes, K., McEvoy, T. G., Butterwith, S. C., Gutierrez, C. G., Carolan, C. *et al.* Epigenetic change in IGF2R is associated with fetal overgrowth after sheep embryo culture. *Nat. Genet.* **27,** 153–154 (2001).
92 Sato, A., Otsu, E., Negishi, H., Utsunomiya, T. & Arima, T. Aberrant DNA methylation of imprinted loci in superovulated oocytes. *Hum. Reprod.* **22,** 26–35 (2007).
93 Hiura, H., Okae, H., Miyauchi, N., Sato, F., Sato, A., Van De Pette, M. *et al.* Characterization of DNA methylation errors in patients with imprinting disorders conceived by assisted reproduction technologies. *Hum. Reprod.* **27,** 2541–2548 (2012).
94 Kobayashi, H., Sato, A., Otsu, E., Hiura, H., Tomatsu, C., Utsunomiya, T. *et al.* Aberrant DNA methylation of imprinted loci in sperm from oligospermic patients. *Hum. Mol. Genet.* **16,** 2542–2551 (2007).
95 Poplinski, A., Tüttelmann, F., Kanber, D., Horsthemke, B. & Gromoll, J. Idiopathic male infertility is strongly associated with aberrant methylation of MEST and IGF2/H19 ICR1. *Int. J. Androl.* **33,** 642–649 (2010).
96 Chang, A. S., Moley, K. H., Wangler, M., Feinberg, A. P. & Debaun, M. R. Association between Beckwith-Wiedemann syndrome and assisted reproductive technology: a case series of 19 patients. *Fertil. Steril.* **83,** 349–354 (2005).
97 Lim, D., Bowdin, S. C., Tee, L., Kirby, G. A., Blair, E., Fryer, A. *et al.* Clinical and molecular genetic features of Beckwith-Wiedemann syndrome associated with assisted reproductive technologies. *Hum. Reprod.* **24,** 741–747 (2009).
98 Mackay, D. J., Boonen, S. E., Clayton-Smith, J., Goodship, J., Hahnemann, J. M., Kant, S. G. *et al.* A maternal hypomethylation syndrome presenting as transient neonatal diabetes mellitus. *Hum. Genet.* **120,** 262–269 (2006).
99 Boonen, S. E., Pörksen, S., Mackay, D. J., Oestergaard, E., Olsen, B., Brondum-Nielsen, K. *et al.* Clinical characterisation of the multiple maternal hypomethylation syndrome in siblings. *Eur. J. Hum. Genet.* **16,** 453–461 (2008).
100 Turner, C. L., Mackay, D. M., Callaway, J. L., Docherty, L. E., Poole, R. L., Bullman, H. *et al.* Methylation analysis of 79 patients with growth restriction reveals novel patterns of methylation change at imprinted loci. *Eur. J. Hum. Genet.* **18,** 648–655 (2010).
101 Demars, J. & Gicquel, C. Epigenetic and genetic disturbance of the imprinted 11p15 region in Beckwith-Wiedemann and Silver-Russell syndromes. *Clin. Genet.* **81,** 350–361 (2012).
102 Mackay, D. J., Callaway, J. L., Marks, S. M., White, H. E., Acerini, C. L., Boonen, S. E. *et al.* Hypomethylation of multiple imprinted loci in individuals with transient neonatal diabetes is associated with mutations in ZFP57. *Nat. Genet.* **40,** 949–951 (2008).
103 Boonen, S. E., Hahnemann, J. M., Mackay, D., Tommerup, N., Brøndum-Nielsen, K., Tümer, Z. *et al.* No evidence for pathogenic variants or maternal effect of ZFP57 as the cause of Beckwith-Wiedemann Syndrome. *Eur. J. Hum. Genet.* **20,** 119–121 (2012).
104 Quenneville, S., Verde, G., Corsinotti, A., Kapopoulou, A., Jakobsson, J., Offner, S. *et al.* In embryonic stem cells, ZFP57/KAP1 recognize a methylated hexanucleotide to affect chromatin and DNA methylation of imprinting control regions. *Mol. Cell.* **44,** 361–372 (2011).
105 Zuo, X., Sheng, J., Lau, H. T., McDonald, C. M., Andrade, M., Cullen, D. E. *et al.* Zinc finger protein ZFP57 requires its co-factor to recruit DNA methyltransferases and maintains DNA methylation imprint in embryonic stem cells via its transcriptional repression domain. *J. Biol. Chem.* **287,** 2107–2118 (2012).
106 Messerschmidt, D. M., de Vries, W., Ito, M., Solter, D., Ferguson-Smith, A. & Knowles, B. B. Trim28 is required for epigenetic stability during mouse oocyte to embryo transition. *Science* **335,** 1499–1502 (2012).
107 Drenth, J. P. & van der Meer, J. W. The inflammasome–a linebacker of innate defense. *N. Engl. J. Med.* **355,** 730–732 (2006).
108 Meyer, E., Lim, D., Pasha, S., Tee, L. J., Rahman, F., Yates, J. R. *et al.* Germline mutation in NLRP2 (NALP2) in a familial imprinting disorder (Beckwith-Wiedemann Syndrome). *PLoS Genet.* **5,** e1000423 (2009).
109 Murdoch, S., Djuric, U., Mazhar, B., Seoud, M., Khan, R., Kuick, R. *et al.* Mutations in NALP7 cause recurrent hydatidiform moles and reproductive wastage in humans. *Nat. Genet.* **38,** 300–302 (2006).
110 Parry, D. A., Logan, C. V., Hayward, B. E., Shires, M., Landolsi, H., Diggle, C. *et al.* Mutations causing familial biparental hydatidiform mole implicate c6orf221 as a possible regulator of genomic imprinting in the human oocyte. *Am. J. Hum. Genet.* **89,** 451–458 (2011).
111 Zhao, Z., Tavoosidana, G., Sjölinder, M., Göndör, A., Mariano, P., Wang, S. *et al.* Circular chromosome conformation capture (4C) uncovers extensive networks of epigenetically regulated intra- and interchromosomal interactions. *Nat. Genet.* **38,** 1341–1347 (2006).

特集 周産期胎盤の診断病理

間葉性異形成胎盤placental mesenchymal dysplasia (PMD)の診断と原因遺伝子

大場 隆[*1] 片渕秀隆[*1]
副島英伸[*2]

はじめに

間葉性異形成胎盤placental mesenchymal dysplasia (PMD)は，胞状奇胎と類似した嚢胞状変化を呈するが，組織学的にはtrophoblastの異常増殖を認めない稀な胎盤形態異常である．部分胞状奇胎や胎児共存奇胎との鑑別が重要であるとともに，早産，胎児発育不全，胎児死亡を高率に合併する高リスク妊娠でもある．一方，PMD発生原因については，ゲノムインプリンティングの異常やVEGF遺伝子の関与が示唆されている．本稿ではPMDの臨床と原因遺伝子について最新の知見を基に解説する．

Ⅰ．PMDの臨床

1．PMDの疫学

1990年代に入って，超音波断層法にて胎盤の嚢胞状変化を呈し，組織学的に胞状奇胎とは異なる胎盤の形態異常が報告され始めた．diffuse stem villous hyperplasia[1]，placentomegaly with massive hydrops of placental stem villi[2]など，様々な呼称が提唱されてきたが，現在では間葉性異形成胎盤placental mesenchymal dysplasia (PMD)の語が定着している．PMDは稀な病態であり，2007年までの英文文献による症例報告は約70例[3]，また2010年までの本邦における症例報告は30余例だが，実際の頻度は4,000～5,000妊娠に1例と推定され[4]，この病態の認識が広まるにつれて本邦での報告例も増えている．妊娠中の超音波断層法スクリーニングがなく，PMDの疾患概念が普及していなかった時代には，原因不明の巨大胎盤としてPMDの診断に至らなかった症例が相当数あるものと推定される．現在我々は本邦におけるPMD症例の解析を進めており，以下はこれまでに集積した32症例の検討に基づいている．

PMDの児は女児が多いこと，さらにPMDの児の25%がBeckwith-Wiedemann症候群(BWS)を呈することから[5]，PMDの発症にはインプリンティング機構が関与していることが示唆されてきた．この詳細は本稿の後半で触れる．近年，生殖補助医療assisted reproductive technology (ART)がインプリンティング異常症のリスクを増大させている可能性が指摘されているが[6,7]，PMDに関してはその影響は乏しいようである．PMDの発症に関わる因子は今後の大規模な前向き調査で検討される必要がある．

2．PMDの診断

PMDの診断基準は確立していない．娩出された胎盤の肉眼所見から疑われるか，あるいは妊娠初期の超音波断層法で部分胞状奇胎や胎児共存奇胎との鑑別に挙げられることが診断の契機となる(**表1**)．

超音波断層法では胎児が認められ，胎盤は肥厚して実質内に大小不整な嚢胞や管腔様構造を呈する(**図1a,b**)．MRIでは，全体的に肥厚した単葉の胎盤が観察され，内部には大小の嚢胞状構造が散在している．超音波断層法所見はPMDを疑う契機として重要であるが，我々が集積したPMD症例のうち，妊娠初期の超音波断層法で胞状奇胎様の構造を指摘されたものは62.5% (20/32)にとどまっており，超音波断層法で所見がないことはPMDを除外する根拠とはならない．さらに超音波断層法における嚢胞や管腔様構造は妊娠経過とともに目立たなくなる可能性が指摘されている．

我々の検討では，母体血中ヒト絨毛性ゴナドトロピンが異常高値を示した症例は約20%で，いずれも一過性の上昇であり妊娠中期以降には減少した．一方，母体血中α-フェトプロテインは測定が行われた症例

[*1]熊本大学大学院生命科学研究部 産科婦人科学分野
[*2]佐賀大学医学部分子生命科学講座 分子遺伝学・エピジェネティクス分野

0287-3745/14/¥100/頁/JCOPY

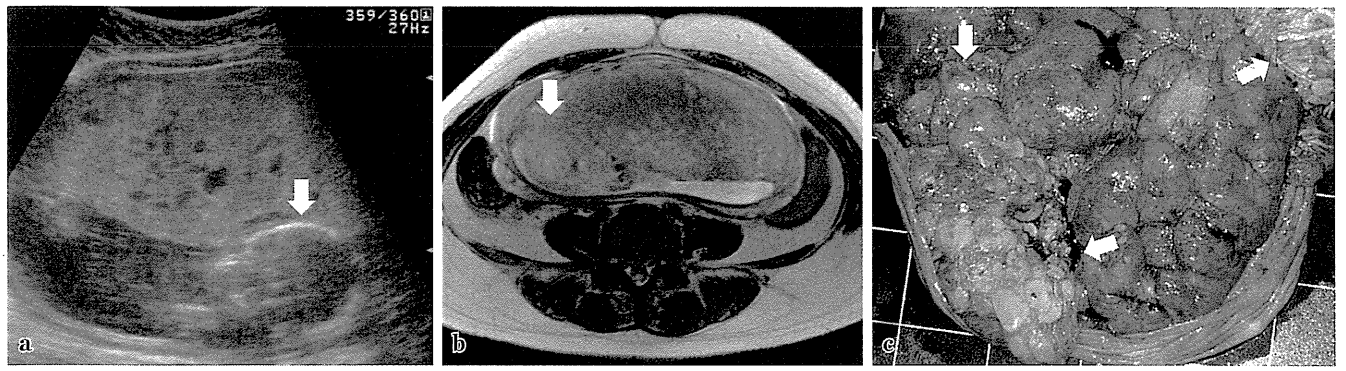

図1　間葉性異形成胎盤(PMD)の画像診断と肉眼所見　a：経腹超音波断層法(妊娠17週5日)，b：MRI T2強調画像(妊娠18週0日)．胎児(矢印)とともに肥厚した胎盤が認められる．胎盤は均質で胎児面は平滑，実質内に大小不整な嚢胞や管腔様構造を認める．c：肉眼所見．妊娠31週2日，出生体重1,116 g，胎盤重量450 g，胎盤胎児重量比0.40．胎盤の胎児面には多嚢胞状の部位(矢印)と変化の乏しい部位が混在している．(北海道大学産科・周産母子センター　山田崇弘博士より提供)

表1　PMDと胞状奇胎の鑑別点(文献3より改変)

	胎児共存奇胎	部分胞状奇胎	間葉性異形成胎盤(PMD)
核型	diploid(正常胎盤＋全胞状奇胎)	triploid	diploid
胎児	正常	三倍体による子宮内胎児死亡	BWS(20%)，胎児発育不全(20%)，子宮内胎児死亡(30%)
母体血中hCG	高値	高値	正常/軽度高値(40%)
母体血中AFP	高値	高値	高値
USG/MRI所見	正常絨毛領域とmultivesicle領域が明瞭に区別される	一様にmultivesicle	巨大な胎盤，multivesicle様の大小不整な管腔
病理組織学所見	trophoblastの異常増殖	trophoblastの異常増殖	幹絨毛血管の動脈瘤様拡張
$p57^{KIP2}$発現	cytotrophoblastに陰性	cytotrophoblastに陽性	絨毛内の間質・血管に陰性
母体続発症	絨毛存続症/絨毛癌	絨毛存続症/絨毛癌	なし

全てが高値を示し，特に第2三半期で高値(各症例の極大値は中央値625 ng/mL(141～7,310 ng/mL))であった．

PMDは一見して巨大な胎盤であることが特徴とされてきたが，PMDでは早産に至ることが多いため，重量が1,000 gを超える，いわゆる巨大胎盤となる症例は約半数にとどまっていた．一方，胎盤/胎児重量比は，中央値0.48(0.23～1.92)と高い値を示しており，相対的な巨大胎盤であることがこの病態を疑わせる指標として重要と考えられる．胎盤の母体面には，一見して胞状奇胎を連想させる多数の嚢胞を認め，その周辺には怒張，蛇行した血管が認められる．このような変化は胎盤の一部または複数箇所に限局して認められることが多い(**図1c**)．

病理組織学評価には，中山の提唱した基準が参考となる[8](**表2**)．水腫様の絨毛には血管がありtrophoblastの異常な増殖はない．蛇行した絨毛血管内に間葉系細胞の増生があり多発性の血栓がみられる．PMDでは$p57^{KIP2}$蛋白は細胞性栄養膜細胞にのみ発現し，絨毛内の間質や血管は$p57^{KIP2}$陰性である[9]．このような病理組織学的所見は同じ胎盤であっても採取部位によって差異が大きく，注意すべき点と思われる．

3. PMDと妊娠異常

図2に我々が集積した症例の在胎週数と出生体重の分布を示す．分娩に至った31症例は，早産83.8%(26/31)，極低出生体重児出生38.7%(12/31)，子宮内胎児死亡intrauterine fetal death(IUFD)16.1%(5/31)，帝王切開率71.0%(22/31)といずれも高率で，PMDの妊娠は高リスク妊娠となることが改めて明らかとなった．BWSの児はBWSを伴わない児に比べると出生体重が大きい傾向はあるが必ずしも巨大児ではなかった．

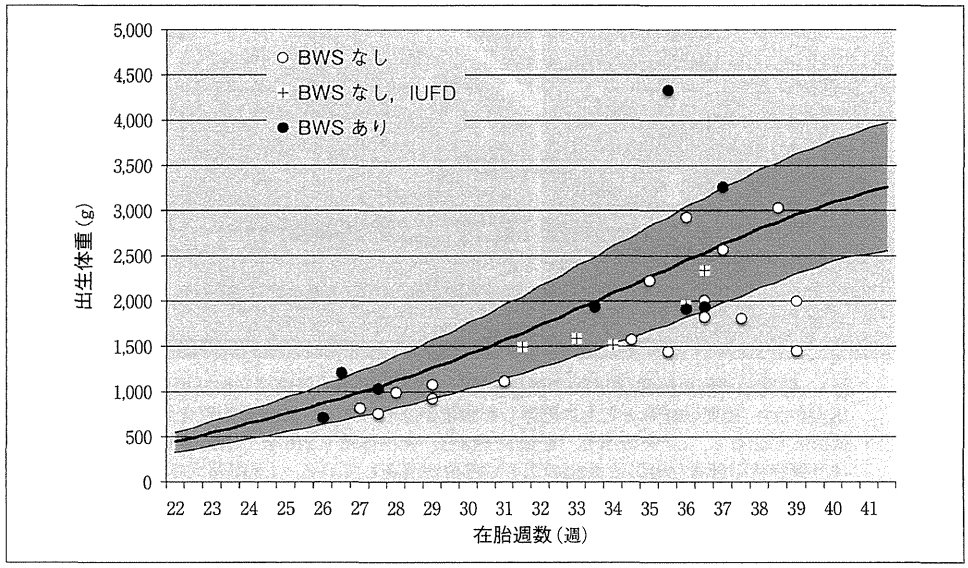

図2　PMD国内症例の在胎週数と出生体重　これまでに我々が集積した本邦のPMD症例のうち，分娩に至った31症例について在胎週数（週）と出生体重（g）の関連を示す．比較のために日本人の胎児発育曲線（m, m±2.0SD）を実線で例示した．週数に比して大きい児（HFD児）は3例で，全てBWSを合併した児であった．週数に比して小さい児（LFD児）は8例であった．出生体重が4,000 gを超える巨大児は1例のみであった．

IUFDは妊娠31～36週に生じており，興味深いことに全てBWSを合併していない症例であった．IUFDの発生率は，1975～2005年における海外症例の35.6%より低率であった．5例中2例が胎児発育不全fetal growth restriction（FGR）を指摘されていたが，出生に至った児と比較しても特にFGRの傾向が強いわけではなかった．IUFDの予知因子を解明することも今後の課題だが，今回集積した症例では，妊娠25週以降に産科的適応でターミネーションが施行された結果，児が救命されていることが多かった．本邦の高リスク妊娠に対する周産期医療提供体制は，PMDにおける児の生存率改善にも有効であると推定される．

表2　間葉性異形成胎盤（PMD）の特徴（文献8より抜粋）

1. 1個の胎盤としての形態を備えている．
2. 肉眼的に部分胞状奇胎に類似する．
3. 血管の走行は蛇行し異形成の外観を呈する．
4. 水腫様変化の絨毛には血管がある．栄養膜細胞の異常増殖はない．
5. 絨毛血管内に間葉系の細胞の増生があり，血管内には多発性の血栓がみられる．
6. 胎児はsmall for dates（子宮内胎児発育遅延）であることが多いが，BWS症例を除き奇形はない．

Ⅱ．PMDの原因遺伝子

1．インプリント遺伝子

インプリント遺伝子とは，一対の対立遺伝子のうち一方の親由来遺伝子のみが発現する（片アレル発現）遺伝子のことで，個体の発生・発育・成長，胎盤形成などに重要な役割を担っている．約25%のPMDにインプリンティング疾患であるBWSを合併することから，BWSの責任領域である11p15領域のインプリント異常の関連が示唆されてきた．11p15には複数のインプリント遺伝子が存在するが，BWSの症状に関連する遺伝子は*IGF2*と*CDKN1C*（$p57^{KIP2}$，*KIP2*）である（**図3a**）．*IGF2*は，細胞増殖を促進するインスリン様増殖因子をコードしており，父性アレルからのみ発現する（父性片アレル発現）．また，*IGF2*は胎盤の成長に重要である．一方，*CDKN1C*は，細胞増殖を抑制するサイクリン依存性キナーゼ阻害因子をコードしており，母性片アレル発現を示す．$p57^{KIP2}$はPMD胎盤の細胞性栄養膜細胞にのみ発現し，絨毛内の間質や血管では発現していないこと[9]，BWSのモデルマウス（$p57^{KIP2}$母性アレル欠失と*IGF2*の両アレル発現（loss of imprinting）を同時にもつ）の胎盤は腫大しPMDに類似した異形成像を示すことから[10]，*IGF2*と$p57^{KIP2}$はPMDの原因遺伝子の候補と考えられている．

PMDは2倍体で，大半は46,XXの核型を示す．2006年頃よりPMDの発症にandrogenetic/biparentalモザイクあるいはキメラが関与する可能性が報告された[11]．androgenetic細胞だけの場合は全胞状奇胎となるが，PMDはbiparental細胞（父由来ゲノムと母由来ゲノムを1セットずつもつ正常細胞）とのモザイクあるいはキメラであり，胎児が存在する．androgenetic細胞の46本の染色体は全て父由来なので，当然なが